DESIGN OPTIMIZATION OF AERODYNAMIC DRAG AT THE REAR OF GENERIC PASSENGER CARS USING NURBS REPRESENTATION

By

Osama Abdul Ghani

A Thesis Submitted in Partial Fulfillment

of the Requirements for the Degree of

Master of Applied Science in Mechanical Engineering

Faculty of Engineering and Applied Science

University of Ontario Institute of Technology

May 2013

Abstract

The rear geometry of a passenger car has the most significant influence on its aerodynamic characteristics. This thesis studied aerodynamic shape optimization of the rear geometry of passenger cars. The Non-uniform rational B-spline (NURBS) curve was used to represent the rear body of a generic passenger car model (the Ahmed Body) and the NURBS parameters were employed for geometry parameterization. These geometry parameters were systematically modified using design of experiments to obtain different geometries of the simplified car model. The computational fluid dynamics (CFD) simulations were performed on these geometries to obtain drag coefficients. Once the results of CFD simulations were available, a response surface model was constructed using linear regression technique. Finally, the design exploration was performed using the response surface model instead of actual CFD simulations. This technique resulted in a radical simplification of the design process as the behaviour of the aerodynamic drag was predicted using a simple polynomial.

The proposed methodology was implemented to perform design exploration of a generic fast back model. The response surface model was able to predict the aerodynamic drag coefficients within an error of 5%. Aerodynamic shape optimization was also performed on a generic notch back model using the response surface technique and the optimized geometry parameters for minimum drag were obtained in only 18 iterations. On the basis of the results, it can be concluded that the proposed methodology is inexpensive, simple and robust. It can therefore provide the basic framework for the design and development of low drag passenger cars.

Dedication

I would like to dedicate this thesis to my loving and supportive parents.

Acknowledgements

First of all, I would like to thank the all mighty Allah, for giving me the knowledge and wisdom and providing me the resources to acquire education. I also want to thank my parents and siblings, specially my elder brother Talha Ghani; without his support and guidance I would not have been able to achieve what I have so far in life.

I also want to express profound gratitude for my research supervisors; Dr. Ahmed Barari and Dr. Martin Agelin-chaab for their expert guidance, moral support and constructive criticism.

Contents

List of Figures

List of Tables

Nomenclature

English symbols

B	Bezier basis function
C	Point on curve
N	NURBS basis function
P	Control point of curve
U	Knot vector of B-spline and NURBS
W	Weigh of control point
C_d	Coefficient of drag
C_f	Coefficient of friction
m	Number of knots in knot vector of knot vector
n	Number of control points of curve

p	Degree of curve
u	Parameter value
u_i	Cartesian component of mean velocity
u_t	Friction velocity
p_m	Mean pressure
x_i	Cartesian coordinate vector component
y^+	Dimensionless wall distance

Greek symbols

α	Rear window slant angle
β	Regression coefficient
μ	Dynamic fluid viscosity
μ_t	Turbulent viscosity

ρ	Fluid density
κ	Turbulent kinetic energy
ε	Turbulent energy dissipation
δ_{ij}	Kronecker delta

Acronyms

CAD	Computer Aided Design
CAM	Computer aided manufacturing
CFD	Computational Fluid Dynamics
NURBS	Non uniform Rational B-spline
RANS	Reynolds Averaged Navier Stokes
RSME	Root Mean Square Error

Chapter 1: Introduction

1.1 Motivation

In recent years, the improvement in fuel efficiency has become a major factor in passenger car development due to increasing population, global decline in fossil fuel reserves, rising fuel prices and the damaging effects of global warming. The aerodynamic drag of a road vehicle is responsible for a large part of the vehicle's fuel consumption and it can contribute to as much as 50% of the total vehicle fuel consumption at highway speeds (Hucho, 1993). Reducing the aerodynamic drag offers an inexpensive solution to improve fuel efficiency and therefore shape optimization for low drag has become an essential part of the overall vehicle design process (Mayer, 2011). Although the wind tunnels can provide most accurate data and test conditions close to actual road conditions, the large number of design variables and geometric configurations involved at the conceptual stage of vehicle design make wind tunnel experiments very expensive and time consuming. The availability of high performance computers and relatively accurate turbulence models have led to increased use of computational fluid dynamics (CFD) in the development of road vehicles.

Shape optimization using CFD also requires numerous computational evaluations for different design configurations and the process can take many days to reach an optimum solution (Muyl, 2004). The time required for CFD simulations and optimization process depends on many factors including the choice of turbulence model, mesh

resolution, the number of design parameters, the parameterization process as well as the optimization strategy.

1.2 Objective

The objective of this thesis is to develop a framework for passenger car rear geometry aerodynamic shape optimization. This framework will help the car designers and body stylists to cost effectively evaluate the aerodynamic performance of various body designs quickly and efficiently at the conceptual stage of vehicle design process.

To achieve the objective, a simplified two-dimensional (2D) Ahmed body will be employed in this study. The rear geometry of 2D Ahmed body will be parameterized using Non-uniform rational B-spline (NURBS) curves. This is because NURBS provide a single mathematical formulation which can represent all common shapes including free form curves and surfaces (Rogers, 2000).

The process employed for aerodynamic shape design can be a direct or indirect shape optimization. In direct shape optimization approach, the process starts with random combinations of design parameters. An optimization algorithm is used which requires CFD simulation at each iteration to find parameters in the design space for minimum drag (Muyl, 2004). This approach requires large number of CFD simulations and takes significant amount of time to complete the optimization process. On the other hand, in indirect approach, design of experiments method is used to obtain geometries from combinations of design parameters and response surface function is built which describes the aerodynamic behaviour of the entire design space. In this study, latter technique will be employed. Linear regression will be used to obtain a response surface model which

will relate the aerodynamic drag to the NURBS parameters. This response surface model will then be used for design exploration and shape optimization.

1.3 Bluff body

Bluff bodies refer to bodies with blunt bases that cause leading-edge flow separation and the formation of recirculation regions in the near wake of the bluff body (Cooper, 1993). This results in a lower pressure on the back surface of the body and sets up a large difference between the relatively high pressure acting on the front of the bluff body and the lower base pressure. Automotive bodies are considered as bluff bodies moving in close proximity to the ground. It has been established that the pressure drag is a direct consequence of flow separation which occurs primarily at the rear end of the body (Ahmed, 1984). More recently, Morelli (2000) mentioned that pressure drag can contribute to approximately 75% to 85 % of total drag.

1.4 Ahmed body

The important features of flow around a bluff body are the regions of flow separation and recirculation in the wake and even the simple shapes produce complex flow structures. These structures are formed in the vehicle wake, which is the main flow separation region, governing the drag experienced by the body (Hucho, 1993). To achieve the qualitative understanding of the relation between wake structure, pressure distribution, drag and geometric configuration, Ahmed (1984) proposed a simplified car model which could generate main flow features of real vehicles without their geometric details. The simplified car model consists of three parts; fore body, mid-section and rear body. The

edges of the fore body are rounded to avoid flow separation. The midsection is a rectangle with sharp edges. The rear end has interchangeable geometry which can be used to study the effect of different geometric configurations on aerodynamic drag and pressure distribution. In the experiments conducted by Ahmed et al. (1984), nine interchangeable rear bodies with different base slants from 0^o to 40^o were tested. Figure 1 shows the schematic of the original Ahmed body.

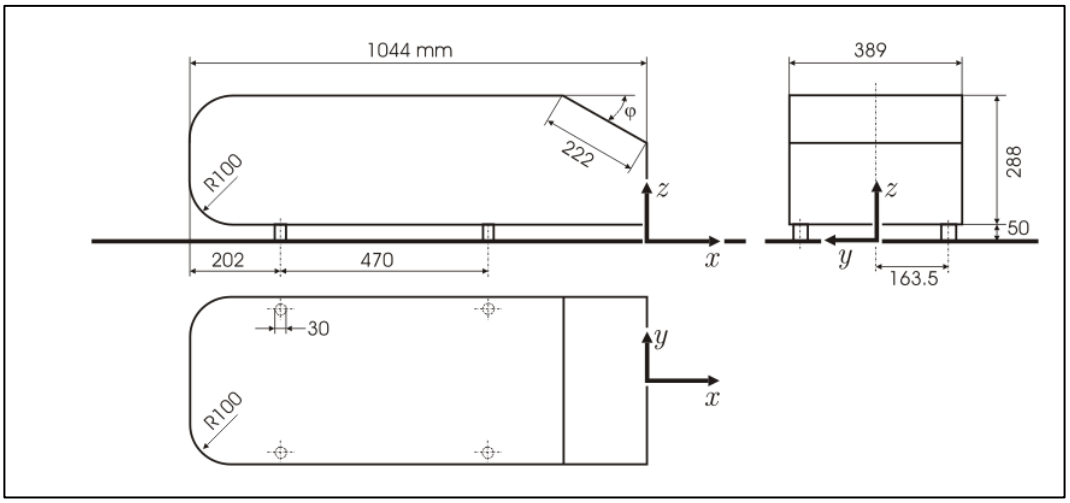

Figure 1: Schematic of Ahmed body (Ahmed, 1984).

1.5 Common rear designs of passenger cars

In passenger car designs, there are three main categories of generic rear geometry: the notch back, the fast back and the square back or station wagon. These generic car bodies and their general wake structure are illustrated in Figure 2. The roof of the notch back drops off at the rear and forms a distinct deck whereas the roof of fast back and square back slopes down continuously at the back. It can also be seen that these generic bodies have distinct wake structures. In the design process, the body stylist selects the type of rear geometry based on vehicle function, design and aesthetics and the role of the

aerodynamicist is to obtain low drag design based on the selected configuration (Hucho, 1993).

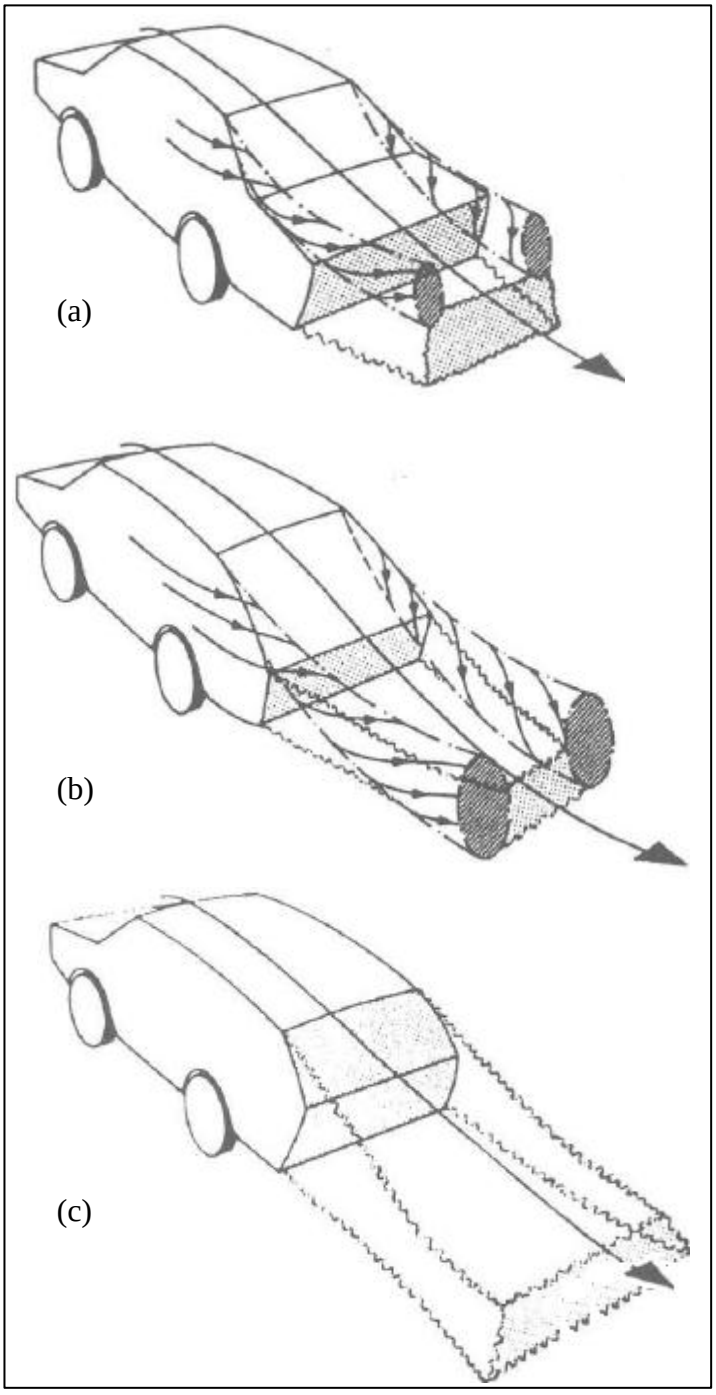

Figure 2: Common generic rear body designs. (a) Notch back, (b) Fast back, and (c) Square back (Hucho, 1993).

Chapter 2: Literature Review

In this section, a brief review of literature is provided on the following topics: description of flow over Ahmed body, drag reduction techniques, car body aerodynamic shape optimization, and use of NURBS for geometry parameterization.

2.1 Flow structure around Ahmed body

The flow over the Ahmed body remains attached on the front and the mid-section and the boundary layer develops on the surfaces of the model. The boundary layer separation occurs at the rear of the model where the flow from the top, bottom and sides separates and forms shear layers. These shear layers curve towards each other and form a closed region with a stagnation point behind the model. This enclosed region of circulating air is called the wake. Although the wake flow of Ahmed body is unsteady, the time averaged flow schematic illustrated in Figure 3 shows important vortex structures that govern the pressure drag produced at the rear end (Ahmed, 1984).

The experiments conducted by Ahmed et al. (1984) investigated the effect of backlight angles in the range of 0^o to 40^o. The backlight angle is the angle of depression of the rear window. In this range, two critical backlight angles (α) which were identified to have a significant influence on the flow structure were 12.5^o and 30^o. Three ranges of backlight angles were identified which have different aerodynamic effects: $0^o < \alpha < 12.5^o$; $12.5^o < \alpha < 30.0^o$; and $\alpha > 30.0^o$.

In the range of $0^o < \alpha < 12.5^o$, the flow remains attached over the rear window slant and separates at the top and bottom edges of the vertical base. The shear layers from the top and bottom roll towards each other and form two circulating regions *A* and *B* as depicted in Figure 3a. As the backlight angle increases, the upper circulating region becomes more dominant. The shear layers from the vertical sides of the slanted base roll up and form longitudinal vortices *C* as shown in Figure 3a. If the flow remains attached on the slanted base, the strength of vortex *A* and *C* depends on the backlight angle.

In the range of $12.5^o < \alpha < 30.0^o$, the strength of longitudinal vortex *C* increases and the flow becomes increasingly three dimensional. These longitudinal vortices are also responsible for maintaining attached flow over the slanted base. Close to 30^o backlight angle, a separation bubble *D* forms on the slanted base but the flow reattaches close to the top edge of the vertical base as shown in Figure 3b. At this point, the flow again separates and forms two circulating regions *A* and *B* as described previously.

For α greater than 30^o, the flow separates at the top edge of the rear window. The two circulating regions *A* and *B* are again formed in the wake but the separation bubble *D* can no longer be distinguished from *A*, instead, a bigger circulating region is formed which comprises of both *A* and *D*.

2.2 Effect of backlight angle on drag

The trend of drag coefficient over a wide range of backlight angles is shown in Figure 4. The total C_d decreases from 0.250 at 0^o to a minimum value of 0.230 at 12.5^o. The C_d again increases to a maximum value of 0.378 upon further increase in backlight angle to 30^o

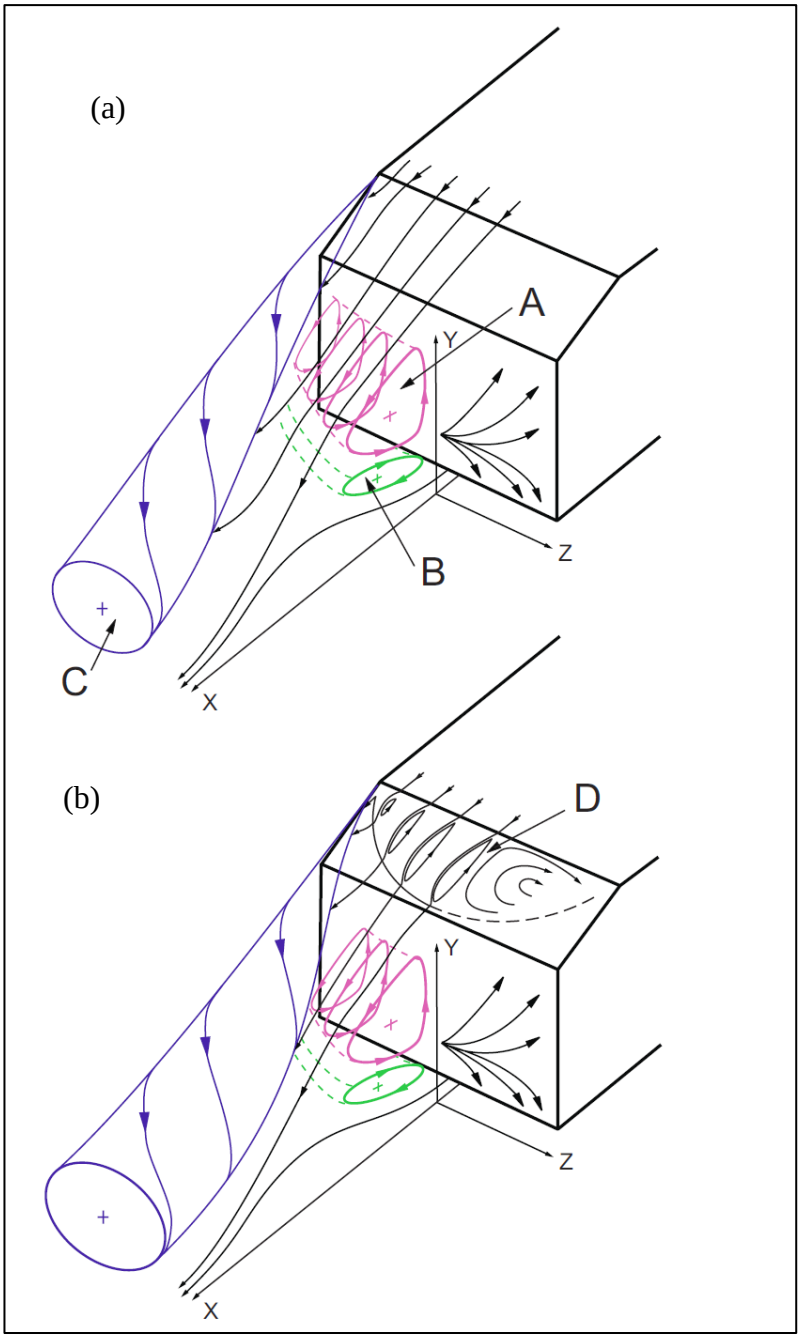

Figure 3: Schematic diagram of flow in the wake of Ahmed body (Ahmed, 1984). (a) $\alpha < 12.5^{o}$ and (b) $0^{o} < \alpha < 12.5^{o}$.

Figure 4 also shows the contributions of different sections of the body to the total drag and it can be inferred that the backlight angle has a significant effect. The relative contribution of drag coefficient (C^{*}_{s} in Figure 3) to the overall pressure drag is most

sensitive to the backlight angle. This suggests that the separation bubble on the slanted base causes a higher pressure force on the model.

It should be noted that the front geometry has little effect on the pressure drag and does not show any significant relation to the backlight angle. This is because the long middle section does not allow any significant interaction of flow between the front and the rear end. In addition, the value of friction drag also does not exhibit any significant relation to the backlight angle. It is reported that the percentage contribution of friction drag to the total drag remains in the range of 15 to 24 percent (Ahmed, 1984).

2.3 Effect of Reynolds number

The experiments conducted by Ahmed et al. (1984) were performed at a wind speed of 60 *m/s.* This corresponds to a Reynolds number of 4.29 million based on model length. Bayraktar (2001) studied the effect of Reynolds number on lift and drag coefficients. The experiments were performed at Reynolds number in the range of 2.2 to 13.2 million. It was observed that over this wide range of Reynolds number, the drag coefficient only altered by 3.5 percent while the lift coefficient altered by 2 percent. Thus it was concluded that the drag coefficient is insensitive at high Reynolds numbers (of the order of 10^6).

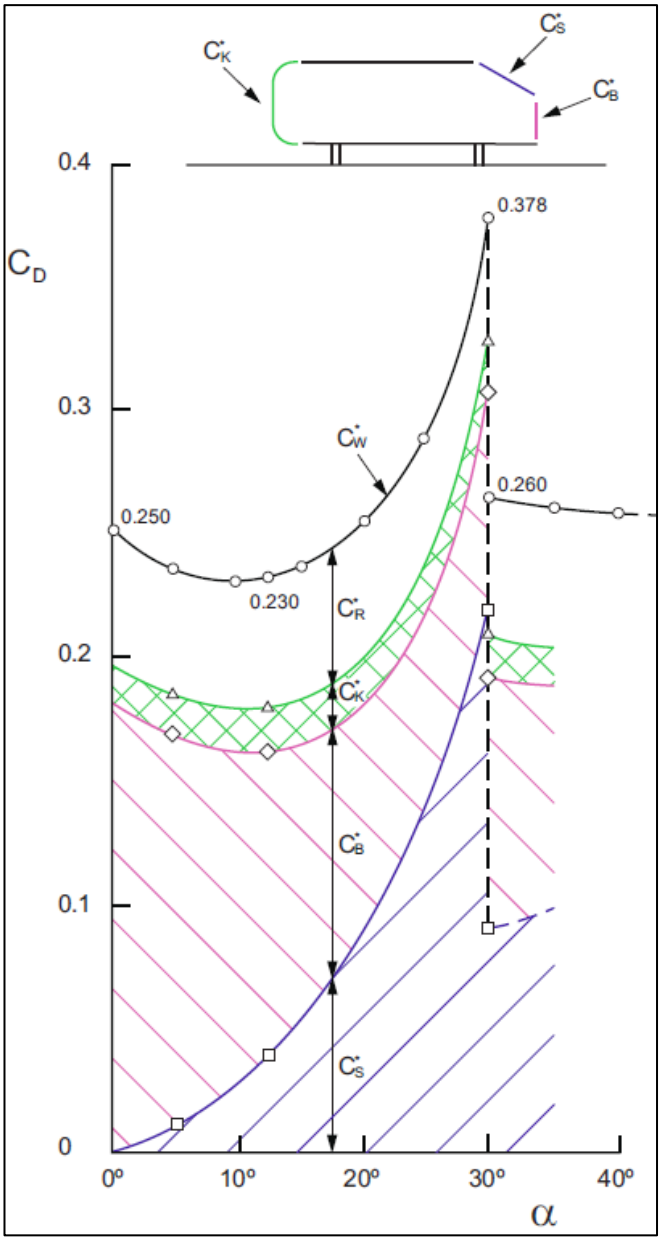

Figure 4: Variation in drag coefficient of the Ahmed body with base slant angle (α) (Ahmed, 1984).

2.4 Computational investigations on the Ahmed body

The Ahmed body lends itself well for CFD studies due to its simple geometry and availability of experimental data. Some difficulties in predicting the overall flow around the Ahmed body using various turbulence models still remains due to the flow separation

on the slant rear window and recirculating region in its wake (Krajnovi´c, 2004). This is partly because the flow in this region is extremely unsteady. Practitioners of CFD strive to develop turbulence models which can predict the real flows as accurately as possible but there is always a compromise between computational cost and accuracy. The availability of high performance computers has enabled the use of highly accurate turbulence models for external flow.

Large Eddy Simulation (LES) is a CFD technique where large flow structures are directly computed from Navier Stokes equations and only the structures smaller than the computational cells are modeled (ANSYS FLUENT user's guide). Since the size of turbulent vortices decreases with increasing Reynolds number, LES is performed at moderate Reynolds numbers so that most of the turbulent vortices can be directly solved rather than modelled. Krajnović (2004) performed LES on 25° Ahmed model with 9.6 and 16.5 million cells for medium and fine grids. These studies were performed at low Reynolds number (2×10^5) to facilitate the use of LES. The results of the study were also validated against the data from Lienhart (2003) and concluded that the flow structure around the model was well predicted.

In addition, Kapadia (2003) performed Detached Eddy Simulation (DES) with a grid size of 1.74 million cells. This study was performed on 25° and 35° Ahmed bodies. The average drag coefficient from DES for both 25° and 35° angles was within 5% of the experimental value reported by Ahmed (1984). Kapadia (2003) also performed unsteady simulations using the Re-normalization group (RNG) k-ε turbulence model. The results suggested that the RNG k-ε model over predicts the drag coefficient. It was also mentioned that the cases where the flow is on the verge of separation or at separation and

reattachment on rear slant as in 25° case pose a strong challenge to computational methods since small difference in separation prediction can lead to substantial difference between CFD and experimental results.

Although the DES and LES have shown superior performance in predicting the overall flow structure, Reynolds averaged Navier Stokes (RANS) equation based turbulence models are chosen for automotive aerodynamics due to limitations of computer RAM and simulation time (Lanfrit, 2005). Braun (2001) used the Realizable k-ε model for simulation of flow on 25° Ahmed body with 2.3 million grid size. The results suggested that although the RANS models do not predict the actual flow separation on the 25° base slant, the overall results including the drag coefficient are predicted with reasonable accuracy.

2.5 Drag reduction techniques

Many attempts have been made since the early years in the automotive industry to reduce aerodynamic drag in order to improve performance and fuel economy. Morelli (1976) developed a theoretical method to determine the shape of passenger car body for minimum drag by imposing the condition that the total lift be zero. With this condition and a gradual variation in the area and shape of transverse cross sections of the body, a basic shape was realized with a drag coefficient of 0.23. This study proved that the aerodynamic drag can be reduced substantially with an optimized body shape without any additional devices.

Later, Morelli (2000) proposed a new technique called “fluid tail” and applied it to the aerodynamic design of basic shape of a passenger car. To achieve a fluid tail, a ring

vortex must be created at the rear of the vehicle. A ring vortex is created behind a body when the flow separation line is perpendicular with respect to direction of motion and the flow separation line coincides with or is very close to the body. The perimeter of the body must be circular or elliptical without any deflection and pressure and velocity must be uniform around the perimeter. To achieve these conditions, the rear wheels were fitted with centrifugal fans which directed the flow around the wheels to the rear body through ducts located at the rear bottom. Wind tunnel tests carried on FIAT Punto 55 showed reduction in drag coefficient from 0.327 to 0.268, a drop by 18 %. The basic criteria proposed by Morelli (1976, 2000) are summarized in Table 1. The idea of fluid tail seems quite promising as it is very much similar to "boat tail" which has been studied in great detail and is well understood (Peterson, 1981). Boat tailing is a technique in which the rear body is tapered which results in pressure recovery at the rear body and reduces pressure drag.

Table 1: Basic criteria for automotive aerodynamic design (Morelli, 2000).

Criterion	**Aim**
Close to zero lift profile	Reduce induced drag
Gradual variation of cross section area and shape of cross section	Reduce pressure drag
Low perimeter/area ratio of cross section	Reduce friction drag

Maji (2007) developed a highly streamlined concept vehicle using only aerofoils. A single piece shell body was developed by placing selected aerofoils at their appropriate locations. The aerofoil integration was terminated at the rear and a B-spline curve was

used to achieve a smooth surface. The total drag coefficient of 0.065 and 0.055 was reported from wind tunnel tests and CFD analysis, respectively.

More recently, Guo (2011) performed aerodynamic analysis of different two-dimensional car geometries using CFD. In the first part of the study, the influence of front body shape was studied. Two models were used; one with sharp edges and the other with smooth rounded edges. Larger stagnation areas were observed on the sharp edged geometry as compared to smooth and rounded edged geometry. Smooth edged geometry also showed reduced pressure areas at bottom of the front end. In the second part of the study, different rear geometries with different backlight angle were studied. The angles considered were 17°, 23° and 30°. With similar front end geometry, the pressure on the front end was greatest for 23º backlight angle and lowest for 17º. The pressure value at the rear end was greatest for 17º and lowest for 30º.

On the other hand, Hu (2011) conducted CFD analysis to study different diffusers with angles of 0^o, 3^o, 6^o, 9.8^o and 12 on a sedan type body. The results showed that the drag coefficient first decreased from 0^o to 6^o and then increased from 9.8^o to 12^o whereas the lift coefficient consistently decreased from 0^o to 12^o. Additional detailed reviews can be found in Gustavsson (2006).

2.6 Aerodynamic shape optimization

Han (1992) performed aerodynamic shape optimization on Ahmad body with three shape parameters: backlight angle, boat tail angle and ramp angle. The k-ε turbulence model CFD solver was coupled to an optimization routine. In this study, an analytic approximation function of the objective function (drag coefficient values from CFD

analysis) was created in terms of the design variables. The optimization was then performed on this approximation function and optimum parameters were found. The CFD analysis was again performed with this optimum set of parameters and the objective function was updated with new results. This process was continued until the parameters for minimum drag were obtained.

The objective function for drag coefficient was represented by the Taylor series expansion:

$$C_D(X) = C_D(X^0) + \Delta C_D(X^0)\delta X + 1/2\delta X H(X^0)\delta X \qquad (1)$$

where X is the vector of design variables; the superscript o represents the nominal design values; $C_D(X)$ is the objective function; $\Delta C_D(X^0)$ is the gradient; and $H(X)$ is the Hessian matrix. The perturbation of design variables δX is given by:

$$\delta X = X - X^0 \qquad (2)$$

Han (1992) approximated the initial objective function from the initial distribution of design variables obtained from the Taguchi orthogonal array. The parameter constraints were backlight angle (0^o to 30^o), boat-tail angle (0^o to 30^o) and ramp angle (0^o to 20^o). The optimization process revealed that the optimum rear body parameters are backlight angle of 17.8^o; boat-tail angle of 18.9^o; and ramp angle of 9.2^o. The determined values for minimum drag were also found to lie within the experimentally determined values of 15-18^o backlight angles, 15-22^o boat-tail angles and 9-14^o ramp angles. The drag coefficient was reduced from 0.209 for a square back to 0.110 for an optimized geometry. It was observed that the optimum geometry produced balanced vertical

recirculation vortices originating from top and bottom surfaces. However, the technique used for parameterization of geometry in this study cannot be applied to complex geometries.

Muyl (2004) used a hybrid method for shape optimization based on genetic algorithm on simplified car-like model. Backlight angle, boat-tail angle, and ramp angle were used as the optimization parameters with optimized values of 23.1º, 13.6º and 23.3º, respectively. Although the work of Muyl (2004) represents a highly sophisticated technology for shape optimization, the computational cost of 250 hours associated with such methods is too high for large scale industrial applications. Moreover, the computational cost for multi objective design optimization which is often required in industrial applications with such method cannot be justified.

Baker (1998) also developed a method to generate and use polynomial approximations for design optimization of an airplane with 28 design variables. A quadratic polynomial was fitted within the variable bounds to the data generated from numerical simulations and the optimization was performed on the quadratic polynomial. The study concluded that the response surface method provides a means to quickly and accurately explore the design space. Later, Krajnović (2009) used polynomial response surface model to optimize the aerodynamic performance of a high speed train. The optimization was performed to improve the shape of the front end of the train for cross wind stability and the dimensions of vortex generators. The results of the study suggested that the response surface method is a practical solution to the complex problem of aerodynamic shape optimization.

2.7 Geometry parameterization using NURBS

Geometry parameterization is an essential part of the design exploration and shape optimization process and there are several methods of generating parametric geometries. A common method of parameterization for automotive bodies is the use of geometric parameters such as edge radius, back light angle and diffuser angle (Han, 1992, and Muyl, 2004). Another method is shape modification by displacing particular edges on the body in the desired direction (Peddiraju, 2009). These parameterization techniques can be implemented in all modern parametric computer aided design (CAD) systems but the drawback of using this parameterization is that only simple shapes with small changes in geometry can be studied.

Non-uniform Rational B-spline curves and surfaces have been used extensively in the aerospace industry for parameterizing complex surfaces of wings and fuselages. The NURBS are the industry standard tool for representing curves and surfaces in CAD, computer aided manufacturing (CAM), and computer graphics. Moreover, NURBS are also used for representing curves and surfaces in initial graphics exchange specification (IGES) which is one of the standard formats for exchange of design information between CAD and CAM software.

Samareh (2004) proposed a free form deformation technique for aerodynamic shape optimization using the NURBS due to its ability to provide a better control over shape changes. The optimization was performed on a fuselage of a business jet and the objective function was the aerodynamic drag coefficient. The NURBS parameters changed in this study were the NURBS control points. The knot vector and the weights of the control

points were kept constant. Lepine (2000) and Bentamy (2002) performed shape optimization of airfoil using NURBS. The design variables in these studies were control points and weights. Lepine (2000) showed that a large number of complex airfoil shapes could be represented using only 13 control points. It was shown that NURBS minimize the number of design variables and provide smooth profiles. Thus, the major advantage of using NURBS is that free form geometrical shapes can be produced with very few design variables. However, the drawback of using NURBS control points as design variables is the difficulty in changing the relative position of control points, which only allows for the control points to be changed in a small range (Song, 2004). In the present work, only the weights of the control points were used for geometric parameterization and it was observed that by careful placement of control points, a large number of geometric variations can be generated.

Chapter 3: Introduction to NURBS

3.1 Introduction to parametric curves

The two common methods for representing curves and surfaces are implicit method and parametric method. The implicit method is a function which depends on physical axis variables that are commonly represented in the form of cartesian (x, y, z) coordinates. In parametric method, the axis variables are defined in terms of an independent parameter and each point on the curve is calculated by a blending function and control points. One major advantage of the parametric curves is the flexibility to produce free form shapes which are either impossible or too complicated to produce using implicit method. The need for parametric curves was mainly derived by the automotive industry to produce free form curves and surfaces for exterior body design. Thus the first method for representing shapes using parametric curves was developed by Pierre Bezier (1970) at Renault Automobile.

Mathematically, parametric Bezier curve of degree *n* is defined by:

$$C(u) = \sum_{i=0}^{n} B_{i,n}(u) P_i \qquad 0 \le u \le 1 \qquad (3)$$

The coefficients P_i are the control point (x, y, z) coordinates and $B_{i,n}$ is the Bezier blending function defined by:

$$B_{i,n} = \frac{n!}{i!(n-i)!} u^i (1-u)^{n-i} \quad 0 \le u \le 1 \qquad (4)$$

A parametric representation of geometry is desired which has local parameterization and can also represent conic curves. The local parameterization means moving the control point does not affect the entire curve. To meet these requirements, a piecewise Bezier curve or B-spline was developed which is constructed from several Bezier curves. These curve segments are joined at breakpoints and the continuity between these segments is defined by the degree of the B-spline.

Mathematically, a B-spline of degree *p* is defined by:

$$C(u) = \sum_{i=0}^{n} N_{i,p}(u) P_i \qquad 0 \le u \le 1 \qquad (5)$$

The coefficients P_i are the control points (x, y, z) coordinates and $N_{i,p}$ is the B-spline basis function defined by:

$$N_{i,0}(u) = \begin{cases} 1 & if\ u_i \le u \le u_{i+1} \\ 0 & otherwise \end{cases} \qquad (6)$$

$$N_{i,p}(u) = \frac{u-u_i}{u_{i+p}-u_i} N_{i,p-1}(u) + \frac{u_{i+p+1}-u}{u_{i+p+1}-u_{i+1}} N_{i+1,p-1}(u) \quad 0 \le u \le 1 \qquad (7)$$

The above equations can result in *0/0*; this is defined to be zero.

The breakpoints of the B-spline are defined by knots and the sequence of knots is called a knot vector.

The knot vector is of the form:

$$U = \left[\underbrace{a, \ldots . a}_{p+1}\ u_{p+1}, \ldots \ldots \ldots \ldots \ldots . . u_{m-p+1,}\ \underbrace{b, \ldots . . b}_{p+1}\right] \qquad (8)$$

$$m = n + p + 1 \qquad (9)$$

where $u_i \leq u_{i+1}$, p is the degree of the NURBS curve. The knot vector in Equation 8 consists of *m+1* elements and the and the first (a) and last (b) elements are repeated *p+1* times and usually equal to 0 and 1 respectively.

The one disadvantage of B-splines is that they cannot represent conics exactly and hence a rational B-spline basis function is needed. This basis function forms a more generalized NURBS.

3.2 Mathematical formulation of NURBS

Mathematically, a NURBS of degree *p* is defined by:

$$C(u) = \frac{\sum_{i=0}^{n} N_{i,p}(u) w_i P_i}{\sum_{i=0}^{n} N_{i,p}(u) w_i} \qquad (10)$$

The basis function is the same as defined previously for B-splines in Equation 7 and w_i are the weights of the control points. When the weights of all control points are 1, the resulting curve is a B-spline. The weight of the control point defines how much that control point "attracts" the curve towards itself relative to other control points. Figure 5 shows the effect of changing the weight (h_3) of the control point (B_3). It can be seen that by modifying the weight of just one control point, several different curves can be obtained. This feature of NURBS curves was exploited in this study to generate free form

curves that represent the rear geometry of the passenger car. Moreover, NURBS weights were used as design parameters to obtain parametric geometry which was used for shape optimization. All the NURBS computations presented in this study were performed using the NURBS toolbox by D.M. Spink (2000).

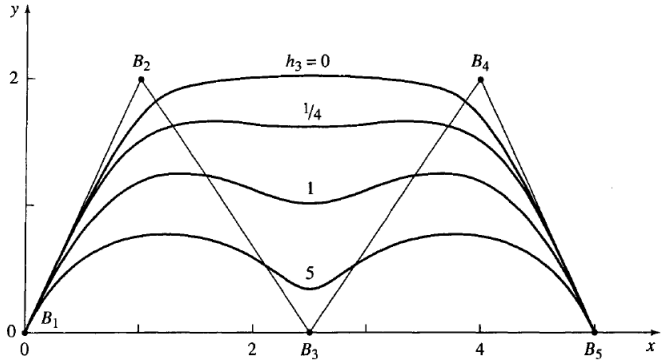

Figure 5: Effect of changing the weight of a control point (Rogers, 2000).

Chapter 4: Response Surface Modelling

4.1 Introduction to response surface modelling

Response surface methodology (RSM) is a set of mathematical and statistical techniques used to develop adequate functional relationship between an objective function *y(x)* and the control or design variables x_1, x_2, x_k. Response surface is a smooth analytical function which is often approximated by lower order polynomials. Mathematically, the approximation can be expressed as:

$$y(x) = f(x) + e, \qquad (11)$$

where $y(x)$ is the unknown function, $f(x)$ is the polynomial function of x and e is the random error. The two most common models used for RSM are 1st degree and 2nd degree model. Since 2nd degree model was used in this study, therefore only 2nd degree model will be discussed here. The model can be expressed mathematically as:

$$y(x) = \beta_0 + \sum_{i=1}^{k} \beta_i x_i + \sum_{i<j} \sum \beta_{ij} x_i x_j + \sum_{i=1}^{k} \beta_{ii} x_i^2 + e \qquad (12)$$

In matrix notation, polynomial response surface can be expressed as:

$$\boldsymbol{Y}(\boldsymbol{X}) = \boldsymbol{X}^T \boldsymbol{b} \qquad (13)$$

where $\boldsymbol{b}$ is the matrix of unknown coefficients:

$$\boldsymbol{b} = (\boldsymbol{X}^T \boldsymbol{X})^{-1} \boldsymbol{X}^T \boldsymbol{Y} \qquad (14)$$

Note that β_0, β_i, β_{ij} are the unknown coefficients determined from the least-square regression which minimizes the sum of the squares of the deviations (SS_E) of predicted values and the actual values obtained from experiments and x_i, x_j are the design variables.

$$SS_E = \sum_{i=1}^{n} \varepsilon^2 = \varepsilon^T \varepsilon = (\boldsymbol{Y} - \boldsymbol{Xb})^T (\boldsymbol{Y} - \boldsymbol{Xb}) \qquad (15)$$

To obtain the polynomial response surface model, a series of experiments need to be performed in which the response variable y is measured for different combinations of control variables.

4.2 Design of experiments

The combinations of control variables are obtained by a systematic procedure called design of experiments. The design of experiments is a concept that uses a set of selected experiments which are performed with the aim of optimizing a process or a parameter and to draw information about the general behaviour of the response/studied object against a set of factors which affect the response. The reason for performing a set of designed experiments is to keep the number of performed experiments as low as possible and to obtain most information with this set of experiments.

4.2.1 Experimental designs

There are various statistical experimental designs which can be categorized in three types: full factorial design, fractional factorial design and composite design.

Full factorial design is a design with all possible combinations of all the design variables. A general practice is to use 2 levels for each variable. Thus, if there are k factors, each at 2 levels, a full factorial design has 2^k runs. This design is generally used for screening of important parameters and to obtain linear models.

Fractional factorial design is a type of design that does not consider all possible combination and uses a fraction of the 2^k combinations. Thus if the number of design factors becomes large, a fractional factorial design can be used. This type of design is also used for screening important factors and for validating the models.

Central composite design consists of a fraction of factorial design combined with centre and axial points which allow the estimation of coefficients for second order models. Each design variable for composite designs can have either 3 or 5 levels.

It's important to note that computer simulations do not have random errors as experienced in physical experiments. The above discussed classical statistical designs account for random errors by spreading the sample points in the design space and taking multiple data points (replication). As stated by Simpson (2001), "classical" notions of blocking, replication and randomization are irrelevant to computer simulation. Thus, for application of design of experiments for CFD simulations, a design of experiment is required which treats all the regions of the design space equally.

4.3 D-Optimal design

A D-Optimal design is one of computer generated designs which addresses the limitations of traditional designs by providing the flexibility to specify the number of

experimental runs and the levels of each design variable. The number of experiments must be equal to or greater than number of unknown coefficients for the specific model being used. Thus, if a quadratic model of 2 factors is required, the number of unknown coefficients is 6 and the design must have at least 6 experiments. (Myers, 2009)

The D-Optimality criterion states that the best combination of design variables in an experiment maximizes the determinant $|\boldsymbol{X}^T\boldsymbol{X}|$ where $\boldsymbol{X}$ is the matrix of design variables with all possible levels of each variable. From statistical perspective, the D-optimal design helps to produce response surface models for which the maximum variance of the predicted response is minimized. Moreover, the D-Optimal design enables more efficient construction of a quadratic response surface model (Alvarez, 2000).

4.4 Model validation and updating

The accuracy of the fitting model can be assessed by various criteria. The most commonly used criteria are R^2 and its adjusted form ${R^2}_a$ which takes into account the number of experiments and degree of freedom.

$$R^2 = 1 - \frac{SS_E}{SS_T} \qquad (16)$$

$${R^2}_a = 1 - \left(\frac{n-1}{n-p}\right)(1 - R^2) \qquad (17)$$

where n is the number of experiments and p is number of regression coefficients. SS_E and SS_T are given by

$$SS_E = \sum_{i=1}^{n} (y_i - \hat{y}_i)^2 \qquad (18)$$

$$SS_T = \sum_{i=1}^{n} {y_i}^2 - \frac{1}{n} (\sum_{i=1}^{n} y_i)^2 \qquad (19)$$

where $\hat{y}$ is the predicted response. The values of R^2 and ${R^2}_a$ are between 0 and 1 and the values closer to 1 signify good fit. Another relevant quantity that measures the accuracy of the fit is the Root Mean Squared Error RSME.

$$RMSE = \left[\sum_{i=1}^{N} \frac{(y_i - \hat{y}_i)^2}{N} \right]^{1/2} \qquad (20)$$

The obtained response surface models must be validated for robustness and accuracy. A common technique is to perform validation experiments over the entire design space and compute the testRMSE. The model can then be improved globally by updating the original experiment data with the test experiments which have high prediction errors. However, this does not guarantee that the region with optimal design is improved. Another approach is to add the data points with the predicted optimal design to the original experiments and update the model. Unfortunately, it is not obvious which method is preferable since it is very much model and problem dependant (Marjavaara, 2006; Sobester, 2004). The flow chart in Figure 6 outlines the procedure for response surface model generation and improvement.

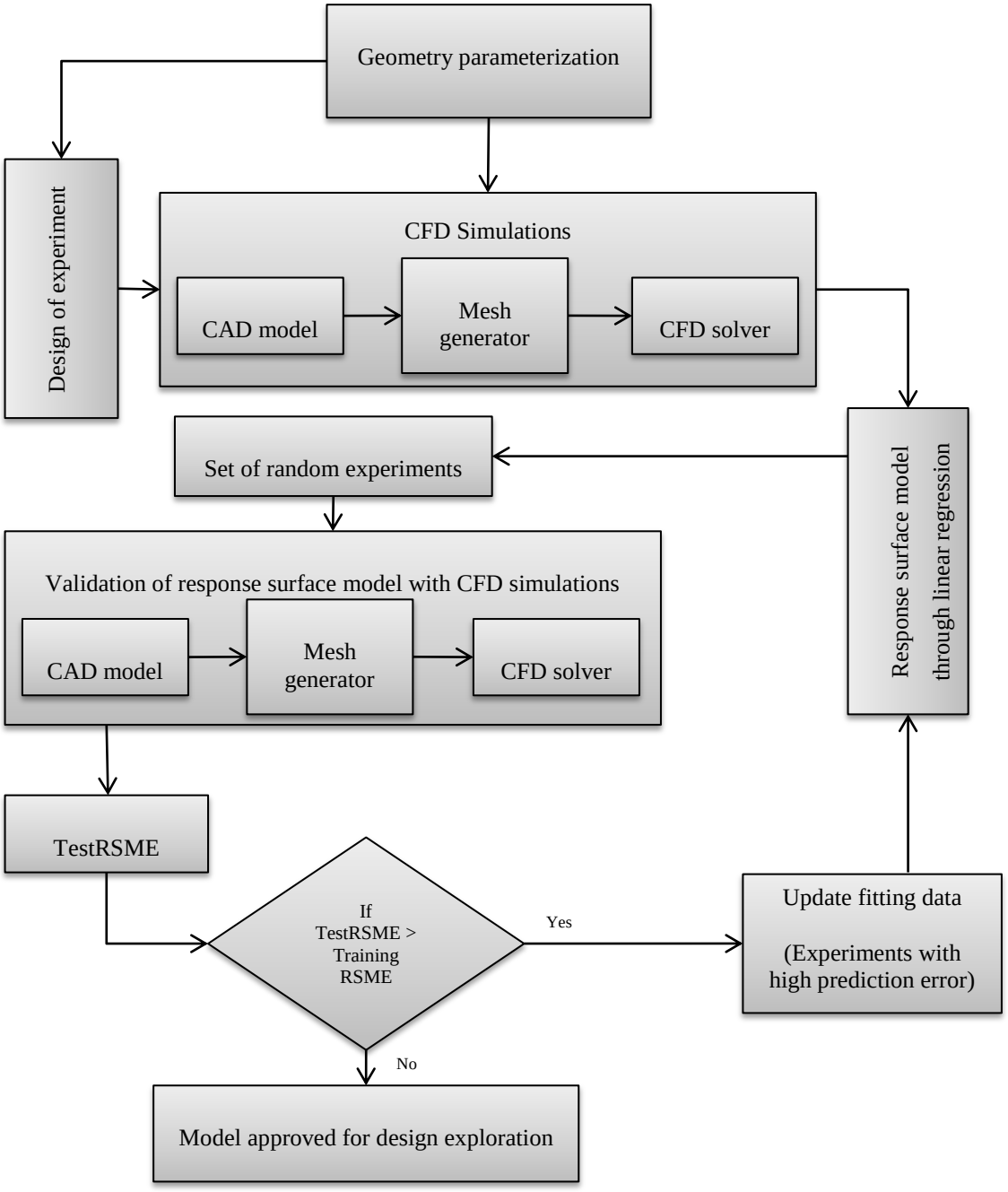

Figure 6: Work flow for generating response surface model.

Chapter 5: Methodology

As discussed in section 1.4, the drag characteristics of car strongly depend on the rear geometry. Therefore, only the rear geometry of Ahmed body was represented with NURBS and parameterized. As mentioned earlier, the weights of control points of NURBS (from here on referred to as NURBS parameters) curve determine how much a control point attracts the curve. The geometry is parameterized with only the weights of control points. This dramatically reduces the number of design variables and the complexity of parameterization. Since the effect of the control point is local, only the part of the curve in the vicinity of the control point is affected. Figure 7 shows the control polygon.

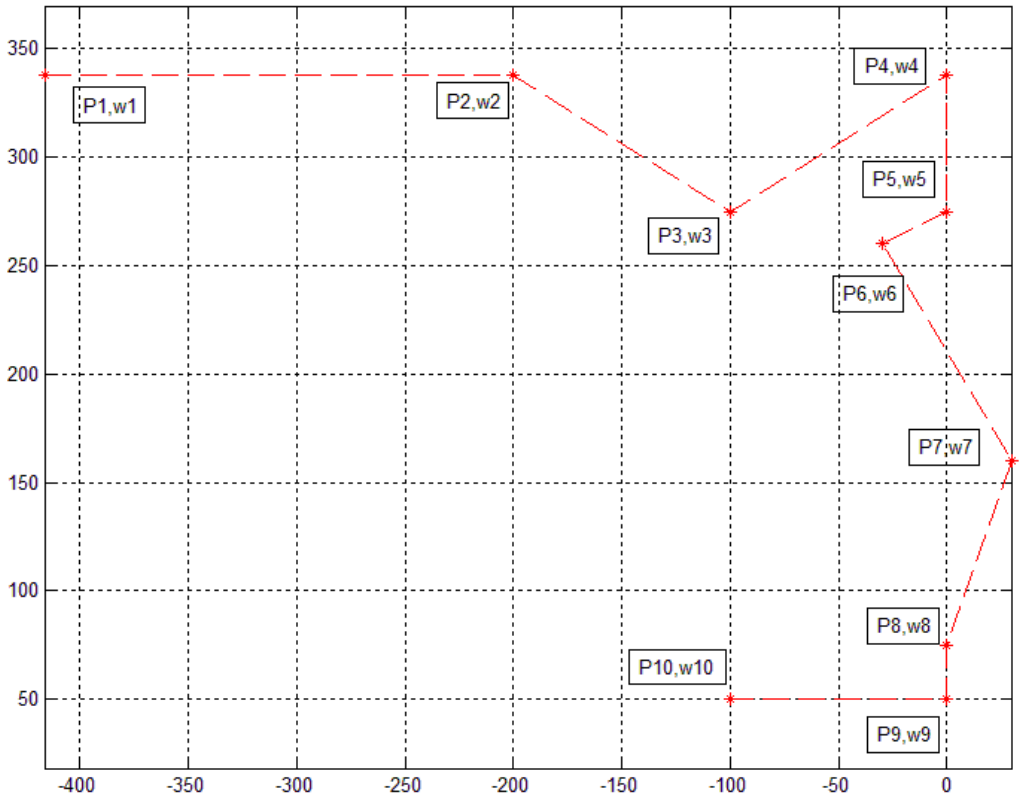

Figure 7: Control polygon of the NURBS curve.

5.1 Geometry parameterization

The rear body of Ahmed model was represented using 10 control points (P_1 to P_{10}). The number of control points was chosen so that the main features of fast back and notch back car model could be obtained. The positions of control points were chosen such that a large variety of shapes could be obtained by changing the NURBS parameters, without the need to change the position of any control point. The weights of the end points w_1 and w_{10} were 1 in all cases since this ensured that the curve passed through the end points.

From the polygon in Figure 7, standard configurations such as Fast back, Notch back and Square back can be obtained as shown in Figure 8. In the current study, a degree 3 NURBS curve with uniform spacing between knots was used. Thus the knot vector for 10 control points using Equations 8 & 9 in section 3.1 is:

$$U = [0\ \ 0\ \ 0\ \ 0\ \ 0.1429\ \ 0.2857\ \ 0.4286\ \ 0.5715\ \ 0.7143\ \ 0.8571\ \ 1\ \ 1\ \ 1\ \ 1]$$

5.2 Model setup

ANSYS Workbench is a commercial package which provides seamless work flow for CFD simulations and was used for all aspects of this research; from CAD model creation to meshing and CFD simulations. CAD model was created in ANSYS Design modeller, computational grid was generated in ANSYS Meshing and, CFD simulations were performed in ANSYS FLUENT. All these software are available in one package as ANSYS Workbench. Figure 9 shows a general work flow for CFD simulation in Workbench.

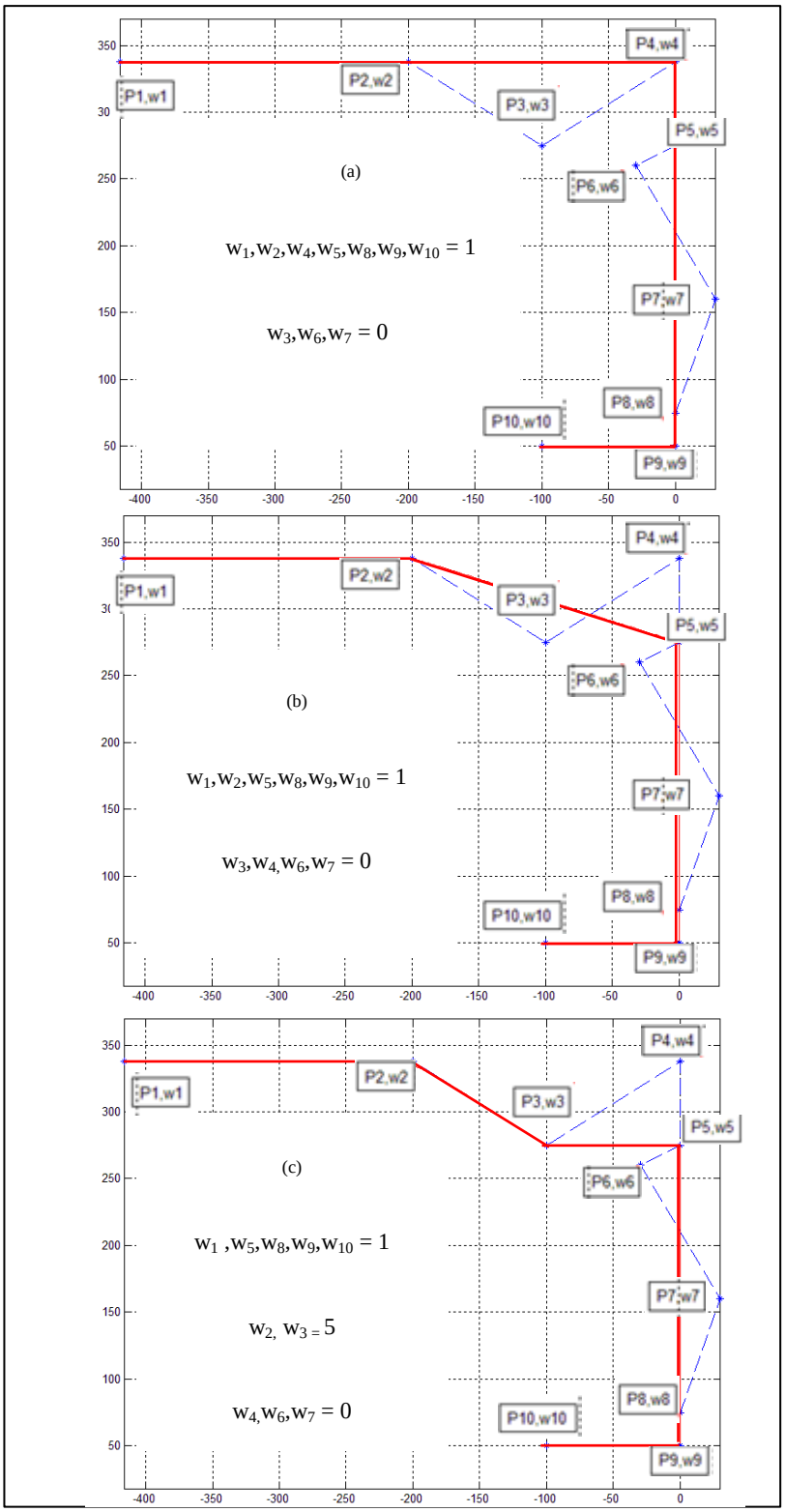

Figure 8: NURBS curve representation of (a) Square back, (b) Fast back, and (c) Notch back.

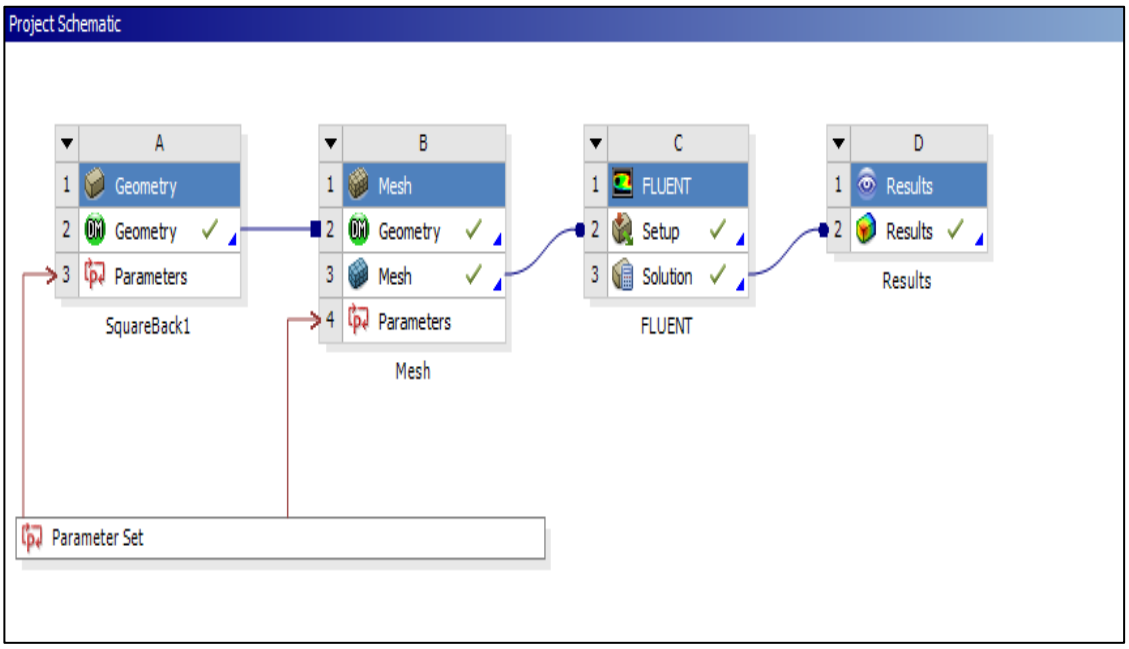

Figure 9: Work flow of CFD simulations in ANSYS Workbench.

5.3 CAD model

The rear geometry created in MATLAB using NURBS toolbox was imported to ANSYS Design modeller and attached to the front end of the Ahmed body. The total length (L) and height (H) of the simplified 2D car model were $1.044m$ and $0.288m$ respectively. The fluid volume was then created around the model. Figure 10 shows the steps involved in creating 2D CAD model.

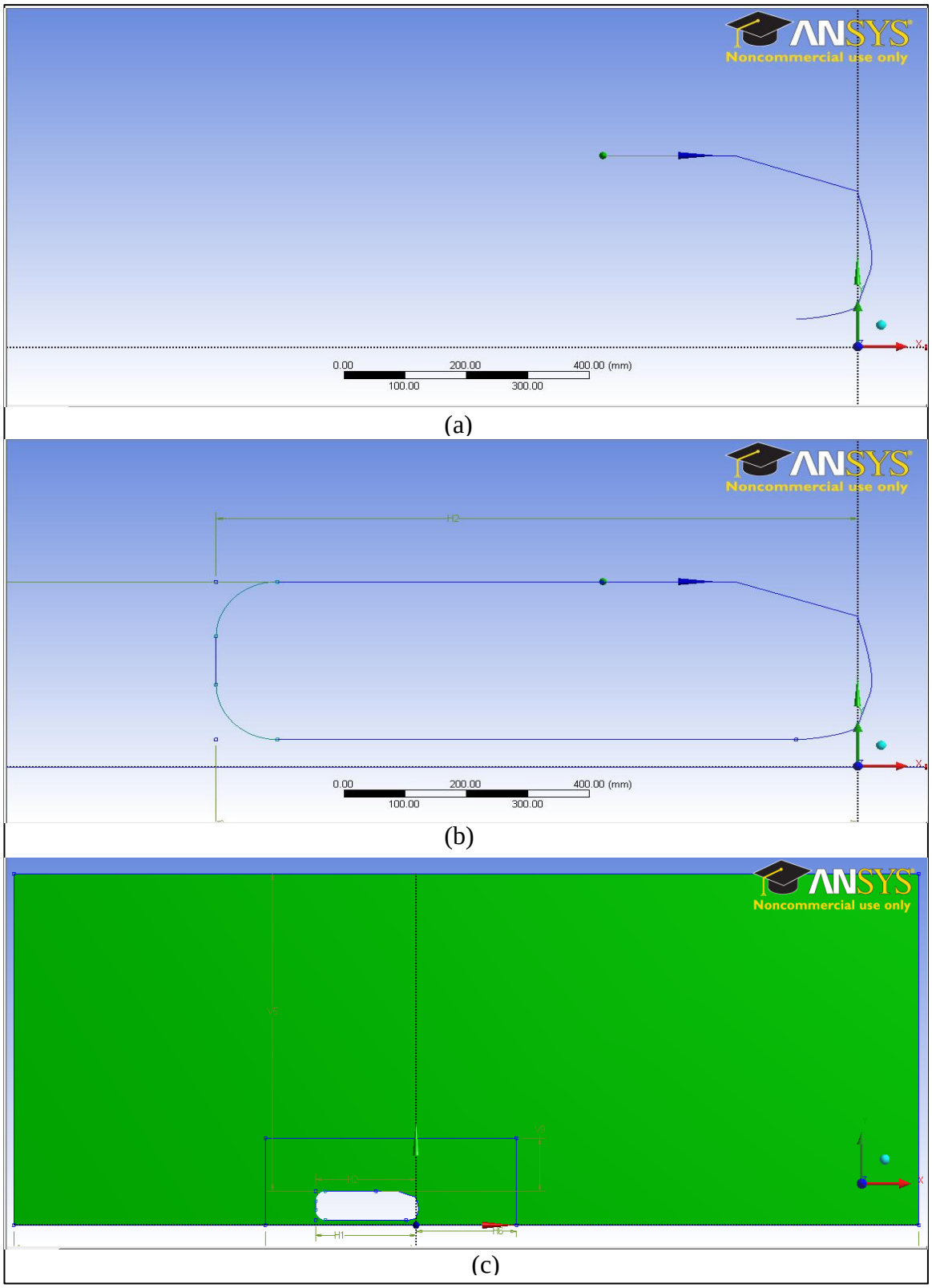

Figure 10: Steps involved in CAD model preparation. (a) Rear geometry, (b) car geometry, and (c) complete CAD model.

Chapter 6: Numerical Modelling

In this research, CFD was used to perform flow analysis on a generic car body. CFD uses numerical methods to solve fluid flow problems. There are different aspects related to CFD application which are discussed in this section.

In order to simplify the problem and reduce computational resources, a two-dimensional computational domain was considered. To ensure that the domain was sufficiently large for this simulation, the best practice guidelines for automotive external aerodynamics (Lanfrit, 2005) were followed. The domain inlet was 3 model lengths upstream of the model and outlet was 5 model lengths downstream. Thus the total domain was therefore 9 model lengths long. The domain far field was 3 model lengths above the model and the total domain height was 3.3 model lengths. Figure 10c shows the complete computational domain.

6.1 Computational mesh

ANSYS meshing software in ANSYS workbench package was used for meshing. Once the parameters for meshing are set, the software detects the changes in geometry from CAD model and creates the mesh automatically. Unstructured, non-orthogonal grid with quadrilateral elements was used to create the computational domain. The accuracy of the computational results and the required time directly depend on the number of cells in the computational domain. The size of the cells near the model should be adjusted such that the wall functions remain valid and the boundary layer should be adequately resolved. Thus a dense mesh is required close to the model and a coarse mesh can be used

away from the model. This strategy to divide the computational domain in coarse and fine regions drastically reduces the total cell count and computational time.

The height of the first wall adjacent cell on the car model was 2 mm and boundary layer was resolved with 5 inflation layers (prism elements) with a growth ratio of 1.2%. The maximum edge length on the model was 5 mm. This ensured high quality mesh on the model. To capture the recirculation region in the wake of the model and the stagnation at the front, a grid refinement region was created with a maximum size of 5 mm elements which extended 0.5 model lengths upstream and above the model and 1.5 model lengths downstream. Element size of 50 mm was used with 1.2% growth ratio in the rest of the domain. This ensured high quality computational domain with a total number of approximately 50,000 elements. Figure 11 shows the details of the computational mesh.

6.2 Mathematical modelling

In this study, the flow is considered to be two-dimensional, incompressible, steady, and turbulent. The fluid is Newtonian with constant density, ρ and dynamic viscosity, μ. The Reynolds Averaged Navier-Stokes (RANS) equations for continuity and momentum conservation can be written as:

$$\frac{\partial u_i}{\partial x_i} = 0 \qquad (21)$$

$$\frac{\partial}{\partial x_j}\left(\rho u_i u_j\right) = -\frac{\partial p_m}{\partial x_i} + \frac{\partial}{\partial x_j}\mu\left(\frac{\partial u_i}{\partial x_j} - \rho\overline{u_i' u_j'}\right) \qquad (22)$$

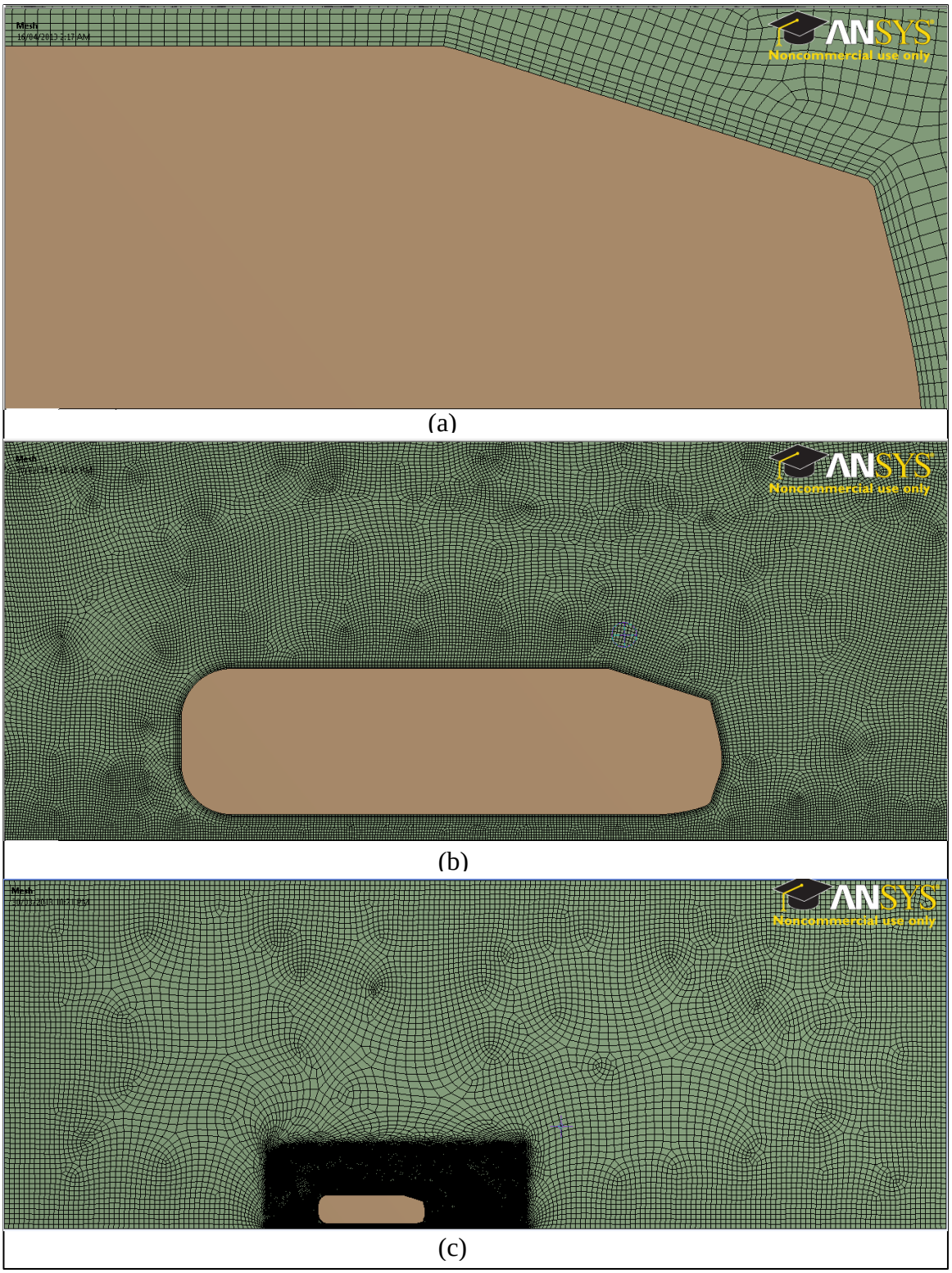

Figure 11: Numerical domain with boundary layer and grid refinement zones.

(a) Boundary layer grid, (b) grid refinement region, and (c) computational mesh.

where $\rho\overline{u_i'u_j'}$ is the Reynolds stress, p_m is the mean flow pressure and u_i is the mean flow velocity in the x_i direction.

The averaging of Navier Stokes equations introduces the additional unknown $\overline{u_i'u_j'}$ Reynolds stress terms which represent the relation between the fluctuating velocities. The closure of Equation 22 requires modelling of these unknown terms. It is important to note that that the turbulence models provide only the average effects of turbulent fluctuations and not the details of turbulence.

There are a number of commercially availble numerical simulation software for solving the RANS equations including Fluent, CFX, StarCD, etc. However, FLUENT is used in this study since it provides fast and accurtate CFD resutls. More over, FLUENT is integated into the ANSYS workbench package which provides a smooth workflow for CFD simulations. A thorough description of computational algorithm can be found in FLUENT manual (ANSYS FLUENT user's guide) and is not repeated here.

6.3 Turbulance model

A common method employed to obtain the closure of the RANS equations is Boussinesq's hypothesis which relates Reynolds stresses to the mean velocity gradients.

$$-\rho\overline{u_i'u_j'} = \mu_t\left(\frac{\partial u_i}{\partial x_j}+\frac{\partial u_j}{\partial x_i}\right)-\frac{2}{3}\rho k\delta_{ij} \qquad (23)$$

where μ_t is the turbulent eddy viscosity and δ_{ij} is the Kronecker delta and k is the turbulent kinetic energy. The *k-ε* turbulence model used in this study is discussed next.

The *k-ε* model is a two equation model which is based on transport equations for turbulent kinetic energy *k* and its dissipation rate *ε*. The *k-ε* model solves the following two equations of turbulent kinetic energy *k* and its dissipation rate *ε:*

$$\frac{\partial}{x_j}(\rho u_j k) = \frac{\partial}{\partial x_j}\left(\left(\mu + \frac{\mu_t}{\sigma_k}\right)\frac{\partial k}{\partial x_j}\right) + P_k - \rho\varepsilon \qquad (24)$$

$$\frac{\partial}{\partial x_j}(\rho u_j \varepsilon) = \frac{\partial}{\partial x_j}\left(\left(\mu + \frac{\mu_t}{\sigma_\varepsilon}\right)\frac{\partial \varepsilon}{\partial x_j}\right) + \frac{\varepsilon}{k}(C_{\varepsilon 1} - \rho C_{\varepsilon 2}\varepsilon) \qquad (25)$$

where P_k is the production term given by:

$$P_k = \mu_t\left(\frac{\partial u_i}{\partial x_j} + \frac{\partial u_j}{\partial x_i}\right)\frac{\partial u_i}{\partial x_j} \qquad (26)$$

and the turbulent viscosity is related to turbulent kinetic energy and dissipation rate by:

$$\mu_t = \rho C_\mu \frac{k^2}{\varepsilon} \qquad (27)$$

The *k-ε* model constants are $C_{\varepsilon 1}$ = 1.44, $C_{\varepsilon 2}$ = 1.92, C_μ=0.09, σ_k =1.0 and σ_ε = 1.3.

6.4 Boundary conditions

The inlet velocity must be specified to obtain the desired value of Reynolds number. A velocity of 40 *m/s* was specified normal to the domain inlet. The Reynolds number based on model length was 2.8 million. In addition, the inlet turbulence intensity was set to 1% and viscosity ratio $\frac{\mu_t}{\mu}$ was set to 3. The turbulence intensity is the ratio of the root-mean-square of the velocity fluctuations to the mean flow velocity. When

turbulence intensity and viscosity ratio are specified, FLUENT solver calculates the dissipation rate using the relation:

$$\varepsilon = \rho C_{\mu} \frac{k^2}{\mu} \left(\frac{\mu_t}{\mu}\right)^{-1} \qquad (28)$$

The outflow condition was specified with zero pressure at the domain outlet. To avoid the effect of shear layers of domain far field on flow field around the model, free-slip wall was specified on domain far field. For car model walls and domain ground, a no-slip boundary condition was imposed.

6.5 Mesh independence test

To ensure that the numerical results were independent of the mesh density, mesh independence tests were performed using three computational grids. Three computational grids with different element sizes in the mesh refinement region as shown Figure 11 were used to estimate the drag coefficient, C_d. Coarse mesh of approximately 30,000 elements, medium mesh of 50,000 elements and fine mesh of 70,000 elements were used. Table 2 summarizes the elements sizes and drag coefficients of different computational grids.

Table 2: Results of mesh independence test.

Mesh	Element size in refinement region	Height of first wall adjacent element	Total elements	C_d
Coarse	10 mm	3 mm	29,783	0.276
Medium	5 mm	2 mm	51,254	0.277
Fine	4 mm	1 mm	72,447	0.279

The change in drag coefficient from the coarse to medium grid was 0.3% and from medium to fine grid was 0.7%. Based on the results of mesh independence test, a medium grid with approximately 50,000 elements was selected for present study to computational time.

6.6 Numerical simulations

FLUENT uses finite volume method to discretize the flow equations. The pressure based coupled solver available in FLUENT was used which solves the momentum and pressure based continuity equations in a coupled manner. This method accelerates the convergence of the solution (Keating, 2011). For better accuracy of solution, second order discretization was used for discretizing the equations of momentum, kinetic energy and its dissipation rate. The convergence of the solution was based on the drag coefficient as well as the residuals of kinetic energy and dissipation rate. The solution was considered to be converged when there was no change in drag coefficient for at least 100 iterations and the residuals of kinetic energy and dissipation rate were less than 10e-8. Moreover, it was also ensured that the dimensionless wall coordinate, y^+ remained in the desired range ($30 < y^+ < 300$) on the car model walls.

6.7 Accuracy of CFD results and mesh resolution

CFD is based on non-linear partial differential equations which attempt to computationally model theoretical and experimental models. The application of CFD for design and analysis is generally categorized into three levels according to the desired levels of accuracy: 1) to provide qualitative information, 2) to provide incremental

quantities, and 3) to provide absolute quantities (Slater, 2008). The level of accuracy desired from CFD results depends on the use of the results. From the perspective of a passenger car design, a conceptual design effort may require only the trends in drag coefficient whereas a detailed design may require accurate determination of the drag coefficient. Since the goal of this study was to obtain the trends in drag coefficients for the development and validation of the proposed framework, qualitative information was required. However, serious attempts were made to minimize error. The sources of errors and uncertainty in CFD results are due to factors such as truncation error between the differential equation solution and the finite equation, spatial discretization scheme, mesh resolution and iterative convergence (Slater, 2008).

A practical method of CFD results accuracy analysis is the grid sensitivity analysis (Mehta, 1991). As shown in Table 2, the grid sensitivity analysis suggests that the change in drag coefficient is less than 1% from coarse grid to fine gird. Therefore a medium grid size of approximately 50,000 elements was used. Moreover it is also crucial to ensure that the dimensionless wall coordinate y^+ is in the desired range of ($30 < y^+ < 300$). This ensures that wall function used in the CFD analysis is valid which in turn strengthens the credibility of CFD results (ANSYS FLUENT user's guide). In this study, the mesh resolution of 2 mm ($1.92\times10e^{-6}$ times the model length) on model walls ensured that the dimensionless wall coordinate y^+ was approximately 150 for all cases. For increased accuracy, second order spatial discretization was used for discretizing the equations of momentum, kinetic energy and its dissipation. The solution of CFD analysis is considered to be converged if the residuals of the governing equations are at least of the order of $10e^{-6}$ (ANSYS FLUENT user's guide). In order to minimize the iteration error, it was ensured

that the residuals decreased to the order of $10e^{-8}$. In addition, the iterations were continued until five significant figures of the drag remained constant for at least 100 iterations. However, the drag coefficients were rounded off to 3 decimal places according to standard practice and consistent with the literature.

Chapter 7: Case Studies

7.1 Design exploration of fast back

For this study, a simple fast back model was considered and the NURBS parameters of rear window slant, the base bulge and the diffuser shown in Figure 12 were used for design exploration and also to obtain different response surface models. By varying the NURBS parameters, the design space of a fast back geometry was explored with D-optimal experimental design. Each parameter had four levels as shown in Table 3.

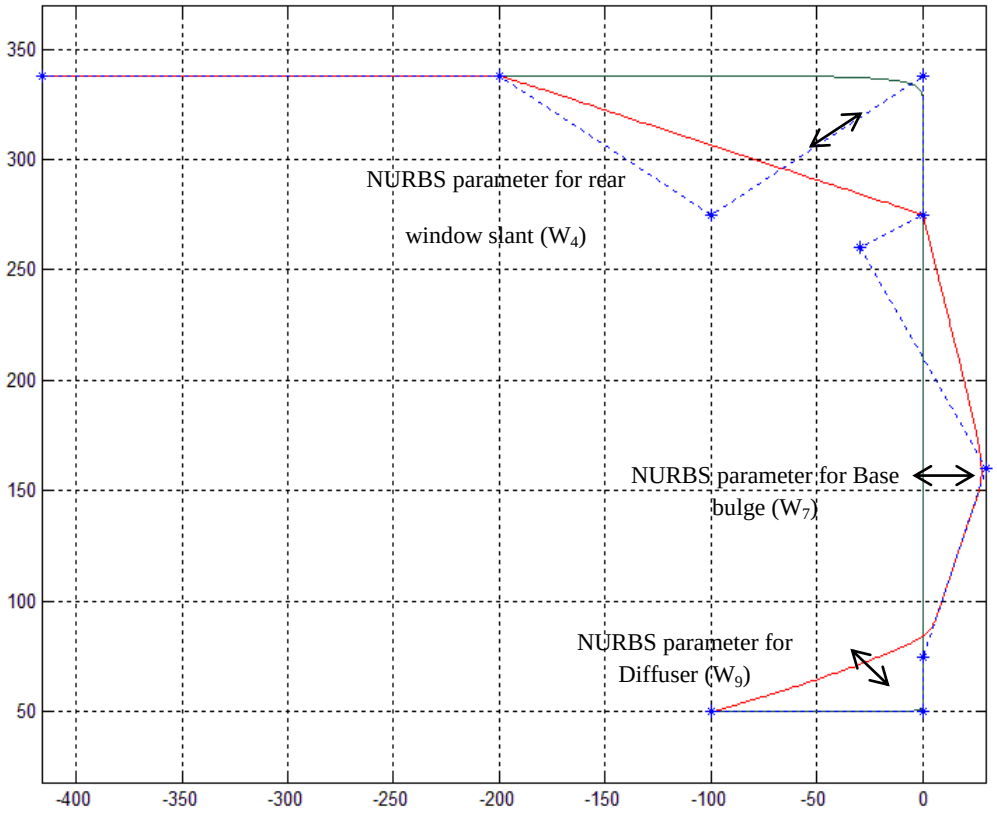

Figure 12: Geometry parameterization for fast back design with three NURBS parameters.

Table 3: Parameter levels for fast back design.

Parameters	Level 1	Level 2	Level 3	Level 4
Rear window slant (W_4)	0	0.05	0.2	1
Base bulge (W_7)	0	0.1	0.3	1
Diffuser (W_9)	0	0.3	1	10

The parameter levels were chosen considering the changes in the geometry they provided and the sensitivity of the curve. Table 4 shows the set of experiments and simulation results for drag coefficient. Figure 13 shows the geometries based on Table 4.

Table 4: Experiment design for fast back with 16 runs.

	NURBS parameters			
Experiment #	**W_4**	**W_7**	**W_9**	**C_d**
1	0	0.3	0.3	0.210
2	0	1	1	0.209
3	0.05	0	0	0.230
4	0.05	0.3	1	0.224
5	0.2	0.1	0.3	0.273
6	0.2	0.3	0	0.277
7	1	0	10	0.341
8	1	0.1	0	0.350
9	1	1	0.3	0.345
10	0	0	0	0.214
11	0	0.1	10	0.209
12	0.05	1	0.3	0.226
13	0.05	0.1	10	0.225
14	0.2	0	10	0.273
15	0.2	1	1	0.272
16	1	0.3	1	0.342

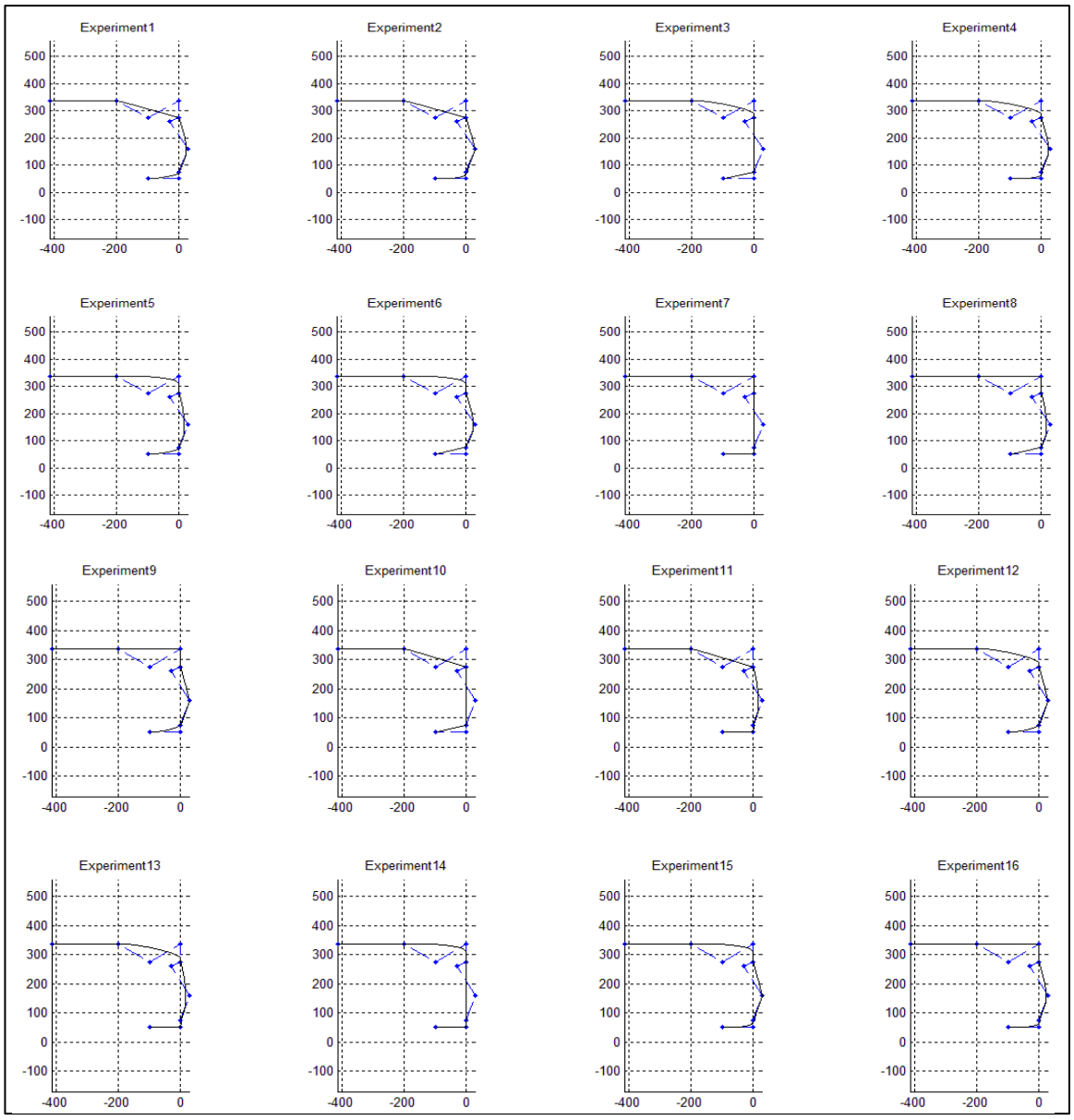

Figure 13: Fast back geometric configurations for CFD simulations.

In this study, only quadratic response surface models were considered since they are appropriate for aerodynamics problems (Krajnović, 2009). With the drag coefficient data obtained from simulations, response surface models were generated in MATLAB using the linear regression of the form in Equation 29.

$$y(x) = \beta_0 + \sum_{i=1}^{k} \beta_i x_i + \sum_{i<j} \sum \beta_{ij} x_i x_j + \sum_{i=1}^{k} \beta_{ii} x_i^2 \qquad (29)$$

where the first term on the right hand side is the intercept, the second is the linear term, third is the interaction term and the fourth is the quadratic term. Response surface models considered were the 'quadratic' model which consists of all the four terms described above and the 'pure quadratic' model which consists of all the terms described above except interaction terms. The quadratic model is given in Equation 30 (Model 1) and pure quadratic model is given in Equation 31 (Model 2).

$$Cd = 0.21308 + 0.36653W_4 - 0.0082266W_7 - 0.0058058W_9 - 0.002776W_4W_7 - 0.00044046W_4W_9 + 0.0014036W_7W_9 - 0.22922W_4^2 + 0.0068434W_7^2 + 0.00053431W_9^2 \qquad (30)$$

$$Cd = 0.21336 + 0.36222W_4 - 0.0050619\ W_7 - 0.0053469W_9 - 0.22762W_4^2 + 0.0040154W_7^2 + 0.0004867W_9^2 \qquad (31)$$

Prediction slice plots in Figure 14 were used to observe the effect of each predictor variable on the response variable. From the slice plots, the relative significance of each predictor variable can also be inferred. It can be observed that the effect of parameter for base bulge (W_7) is insignificant. Thus a simplified model given in Equation 32 (Model 3) was constructed by neglecting the insignificant parameter.

$$Cd = 0.21283 + 0.36222W_4 - 0.0060485\ W_9 - 0.22762W_4^2 + 0.00055988W_9^2 \qquad (32)$$

Table 5 shows the statistics of the models. It can be seen that the removal of W_7 improves the accuracy of the fit. Figure 15 shows the response surface plot of Model 3.

Model 3 was selected for further investigation and additional 50 simulations with 2 parameters were performed to validate Model 3. The parameters were the rear window slant (W_4) and the diffuser (W_9).

Figure 16 compares the drag coefficients from 50 validation simulations and the drag coefficients predicted by Model 3. It can be observed that the predictions of model are very close to actual values. Figure 17 shows prediction error (in percent) of Model 3. The maximum prediction error of the model is 6.8%. Since the model showed good performance over the entire design space, Model 3 was used for design exploration.

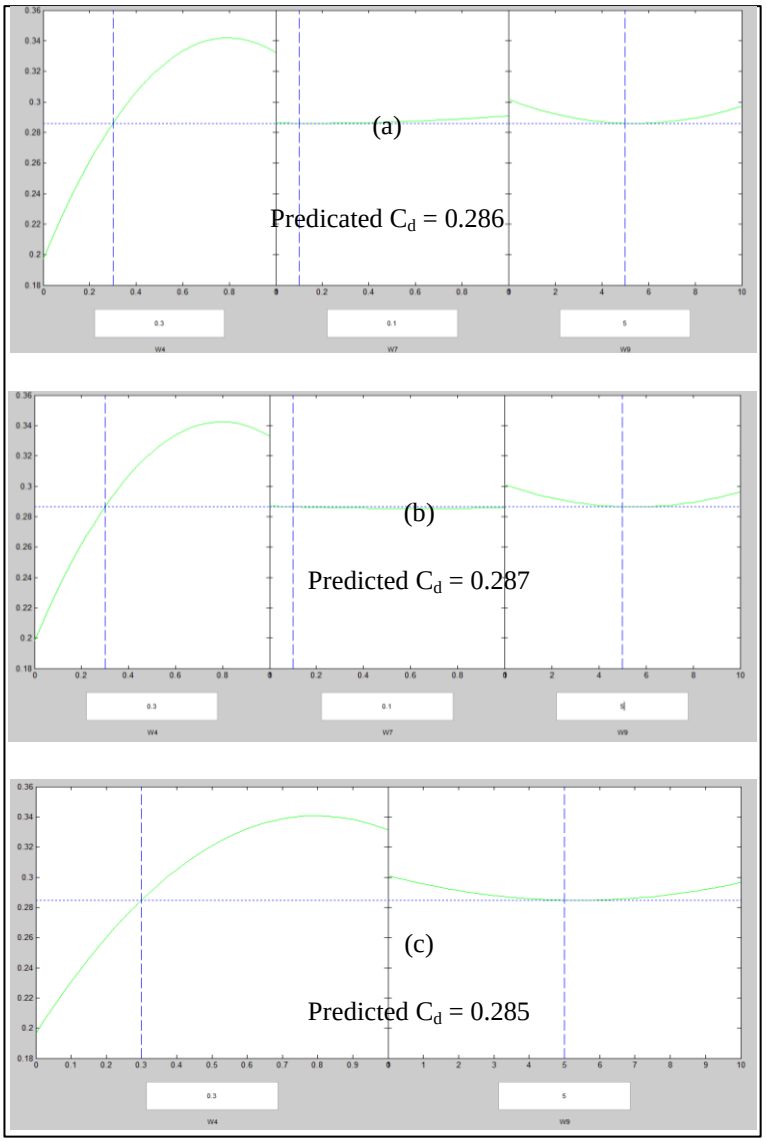

Figure 14: Slice plot of response surface, (a) Model 1, (b) Model 2, and (c) Model 3.

Table 5: Statistics of fitted response surface models.

	R^2	R^2-adj	RMSE
Model 1	0.999	0.999	0.00179
Model 2	0.999	0.999	0.00185
Model 3	0.999	0.999	0.00172

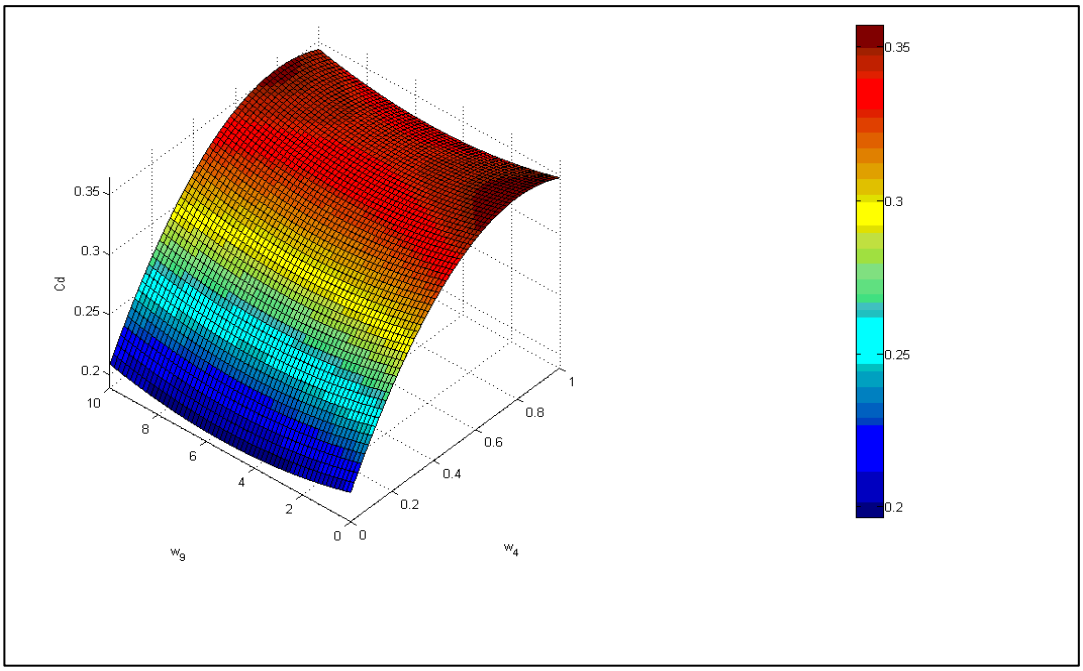

Figure 15: Drag coefficient response surface of Model 3 for fast back.

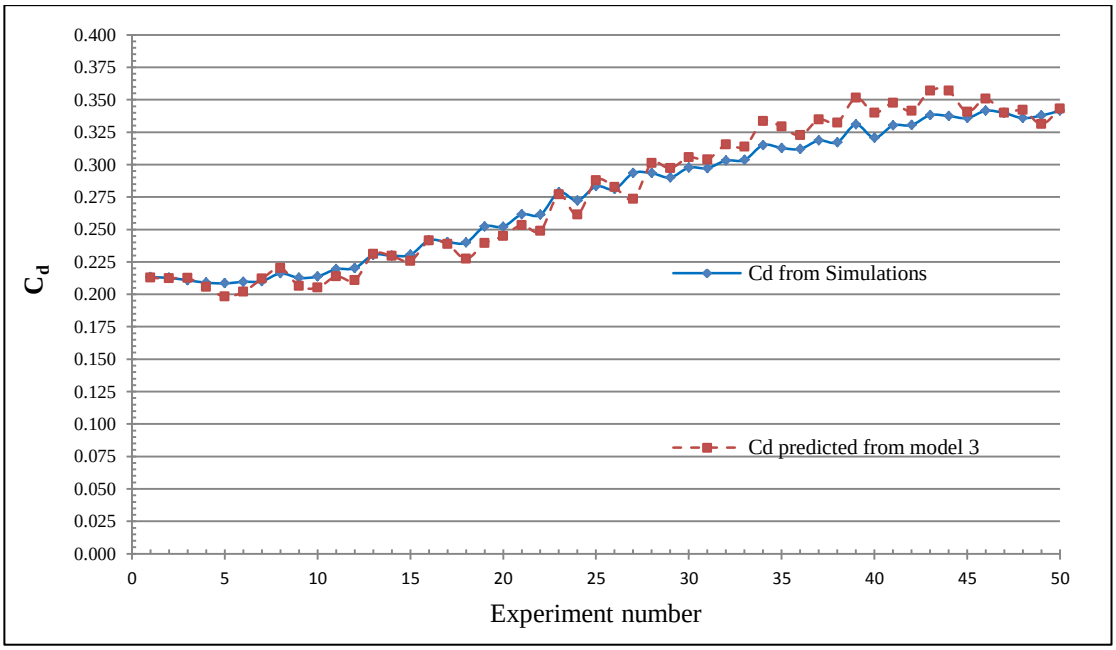

Figure 16: Comparison of simulated and predicted drag coefficients.

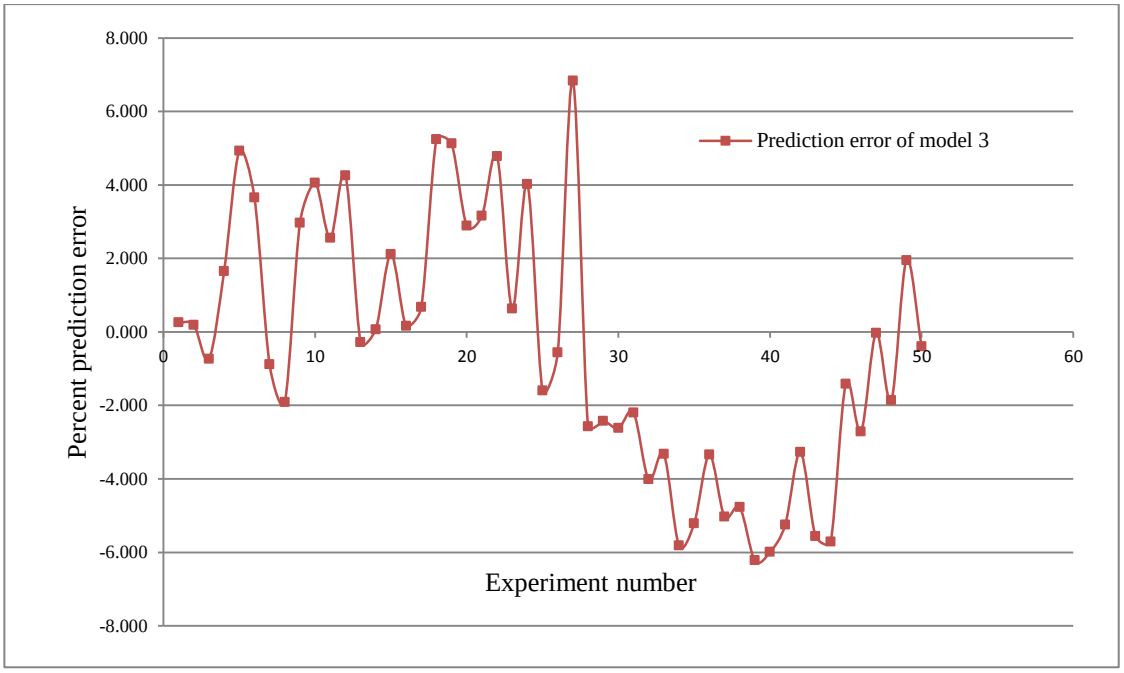

Figure 17: Prediction error of Model 3.

7.1.1 Design exploration

For design exploration, a target drag coefficient was specified and the equation of Model 3 was solved to obtain the required parameters. The geometries were then constructed with the calculated parameters and simulations were performed to validate the solution. Table 6 summarizes the results of design exploration. To ensure the robustness of the model, the target drag coefficients were specified over a wide range. The model was able to predict the drag coefficients within 5% of actual value. Thus it can prove to be an efficient tool for design at the conceptual level of vehicle development when there are several design options. The success of the response surface model also validates the use of NURBS weights as the design parameters.

Table 6: Design exploration results for fast back design.

Model 3 validation	NURBS parameters		target Cd	Simulation Cd	Error (%)
	W_4	W_9			
1	0.154	3	0.250	0.261	4.288
2	0.136	1.5	0.250	0.256	2.350
3	0.2240	8	0.270	0.279	3.323
4	0.7407	5	0.340	0.333	-2.098

The percentage errors of 50 validation experiments for Model 3 shown in Figure 17 suggest that the maximum error of the model is approximately ±6% The errors obtained in design exploration shown in Table 6 are well within this range. In addition, from a detailed mesh independence analysis, it was observed that maximum change in drag coefficient for different mesh sizes for same geometry did not change more that 0.7%. Thus it can be considered that the maximum error of CFD simulations is about 1%. Therefore, it can be inferred that the errors in Table 6 are also composed of 1% error from CFD simulations.

7.2 Shape optimization of a notch back

A notch back is a styling term for automotive body with a trunk whose lid forms a distinct deck. To further study the applicability of proposed geometric parameterization, a simple notch back model was considered and the NURBS parameters of top edge of rear window, bottom edge of rear window, boot lid, the base bulge and the diffuser shown in Figure 18 were used for shape optimization and to obtain response surface model. A quadratic model with interaction terms was not considered since it required greater number of data points. To obtain a pure quadratic model with five variables, a total of

eleven regression coefficients need to be calculated which required at least eleven data points. Moreover, to acquire enough data for the entire design space, each of the five NURBS parameters was studied at 4 levels shown in Table 7. This required a D-optimal array with 16 runs to design the CFD experiments. The drag coefficients obtained from the CFD simulations and the corresponding parameter combinations were then used for linear regression to construct the mathematical model.

Table 7: Parameter levels for notch back design.

Parameters	Level 1	Level 2	Level 3	Level 4
Rear window top edge W2	0.1	0.5	1	5
Rear window bottom edge W3	0.1	0.5	1	5
Trunk lid W5	0	0.2	0.6	1
Base bulge W7	0.1	0.5	1	5
Diffuser W9	0	0.5	2	10

The parameter levels were chosen considering the changes in the geometry they provided and the sensitivity of the curve. Table 8 shows the set of experiments and simulation results for drag coefficient. Figure 19 shows the geometries based on Table 8.

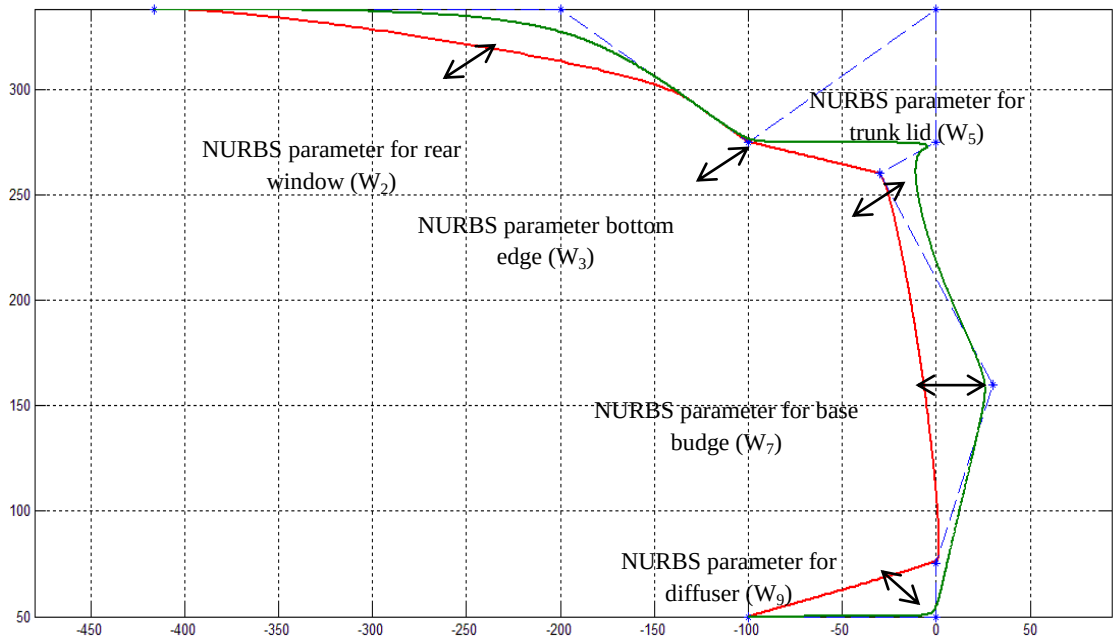

Figure 18: Geometry parameterization for notch back design with five NURBS parameters.

Table 8: Experiment design for notch back with 16 runs.

Experiment #	**NURBS parameters**					**C_d Simulation**
	W_2	W_3	W_5	W_7	W_9	
1	0.1	0.1	0	0.1	0	0.187
2	0.1	0.5	0.2	0.5	0.5	0.236
3	0.1	1	0.6	1	2	0.246
4	0.1	5	1	5	10	0.249
5	0.5	0.1	0.2	1	10	0.229
6	0.5	0.5	0	5	2	0.185
7	0.5	1	1	0.1	0.5	0.239
8	0.5	5	0.6	0.5	0	0.245
9	1	0.1	0.6	5	0.5	0.233
10	1	0.5	1	1	0	0.238
11	1	1	0	0.5	10	0.187
12	1	5	0.2	0.1	2	0.218
13	5	0.1	1	0.5	2	0.229
14	5	0.5	0.6	0.1	10	0.233
15	5	1	0.2	5	0	0.226
16	5	5	0	1	0.5	0.194

A quadratic response model with linear and quadratic terms of the form of Equation 33 was used to obtain Model 1 for the notch back geometry. Table 9 and 10 show the coefficients and statistics respectively of Model 1.

Table 9: Coefficients of terms in Model 1.

Coefficient of	**I**	**W_2**	**W_3**	**W_5**	**W_7**	**W_9**	**W_2^2**	**W_3^2**	**W_5^2**	**W_7^2**	**W_9^2**
values	0.1934	-0.0146	0.0065	0.1403	0.0151	-0.0038	0.0026	-0.0009	-0.0987	-0.0028	0.0004

$$C_d = I + W_2 + W_3 + W_5 + W_7 + W_9 + W_2^2 + W_3^2 + W_5^2 + W_7^2 + W_9^2 \quad (33)$$

Table 10: Statistics of fitted response surface Model 1.

R^2	**R^2-adj**	**trainingRMSE**	**testRSME**
0.924	0.735	0.0112	0.0098

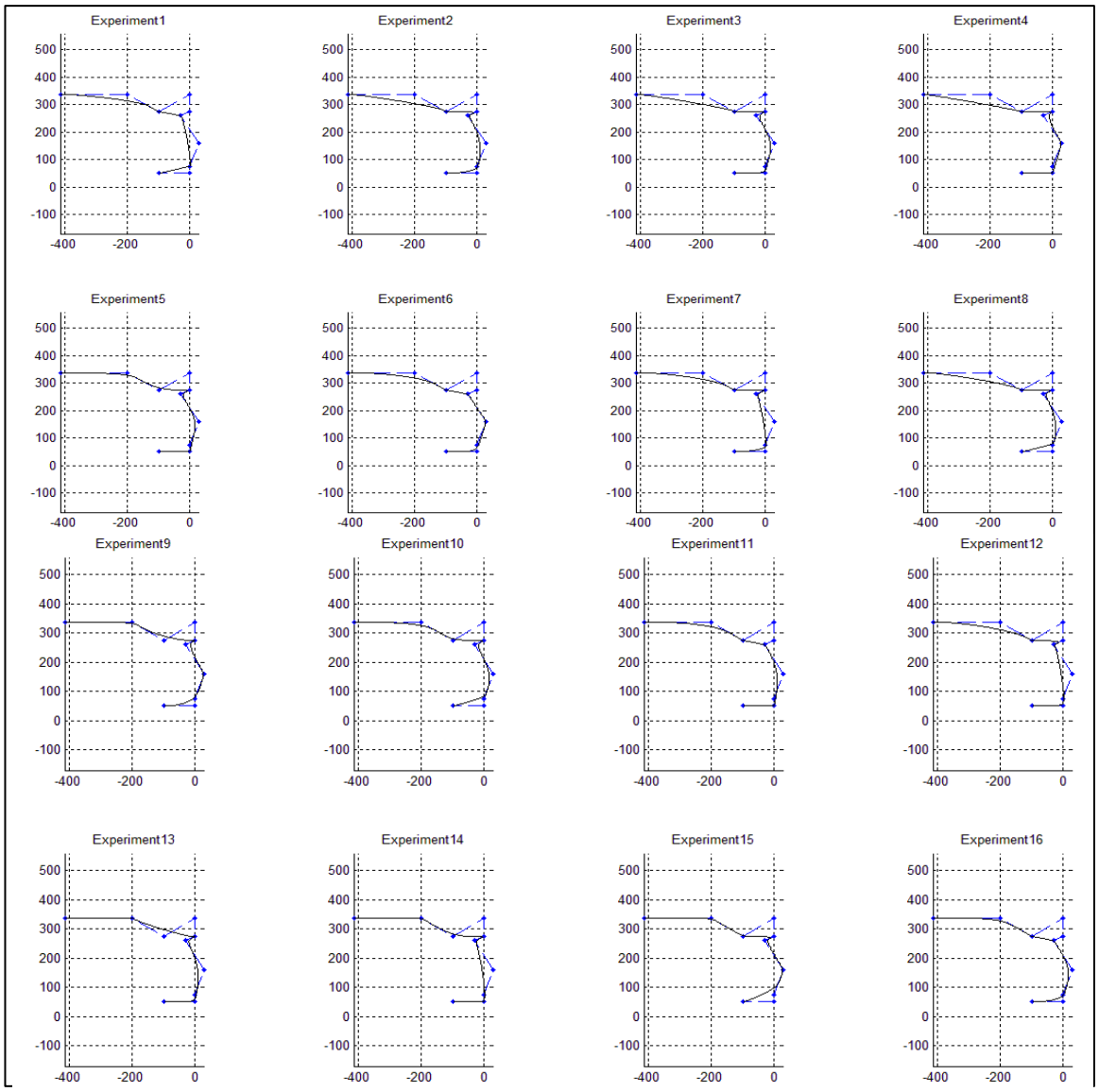

Figure 19: Notch back geometric configurations for CFD simulations for the 16 experiments as indicated.

The obtained pure quadratic model was then validated with additional experiments which were designed to test the entire range of parameters and the testRMSE was calculated dynamically. The validation experiments were performed until the change in testRMSE value was considerably small. For 33 validation experiments, the testRMSE was 0.0098. A model updating scheme as discussed in Figure 5 was applied to reduce the testRMSE and the experiments with absolute prediction error greater than 0.01 were

added to the fitting data. An updated model of the same form of Equation 33 was obtained with regression coefficients shown in Table 11. Table 12 compares the statistics of Model 1 & 2.

Table 11: Coefficients of terms in Model 2.

Coefficient of	I	W_2	W_3	W_5	W_7	W_9	W_2^2	W_3^2	W_5^2	W_7^2	W_9^2
values	0.1966	-0.0023	-0.0044	0.1273	0.0120	-0.0040	0.0002	0.0008	-0.0868	-0.0022	0.0004

Table 12: Statistics of fitted response surface Models 1 & 2.

	R^2	R^2-adj	trainingRMSE	testRSME
Model 1	0.924	0.735	0.0112	0.0098
Model 2	0.834	0.715	0.0107	0.0067

From Table 12, it can be seen that Model 2 is superior since it predicts the drag coefficient more accurately over the entire range of design parameters. Figure 20 shows the prediction error in percent of Model 2. Figure 21 compares the testRMSE of the two models. It should be noted that although the Model 2 shows better performance globally, it does not guarantee good performance in the region of optimal design.

7.2.1 Shape optimization based on response surface model

The shape optimization was performed using the Model 2 obtained in the preceding section. The constrained non-linear optimization solver available in MATLAB was used to minimize the drag coefficient function. The starting point of the optimization was Model 2 with all parameters set to level 1 as given in Table 7 and the variable bounds were all values between level 1 and level 4. Once the values of parameters were obtained for minimum drag, simulations were performed with the optimal design parameters and the initial data was updated with the new data and linear regression was performed again

to update the response surface model. The process was continued until the drag coefficient value converged. The flow chart in Figure 22 shows the optimization process.

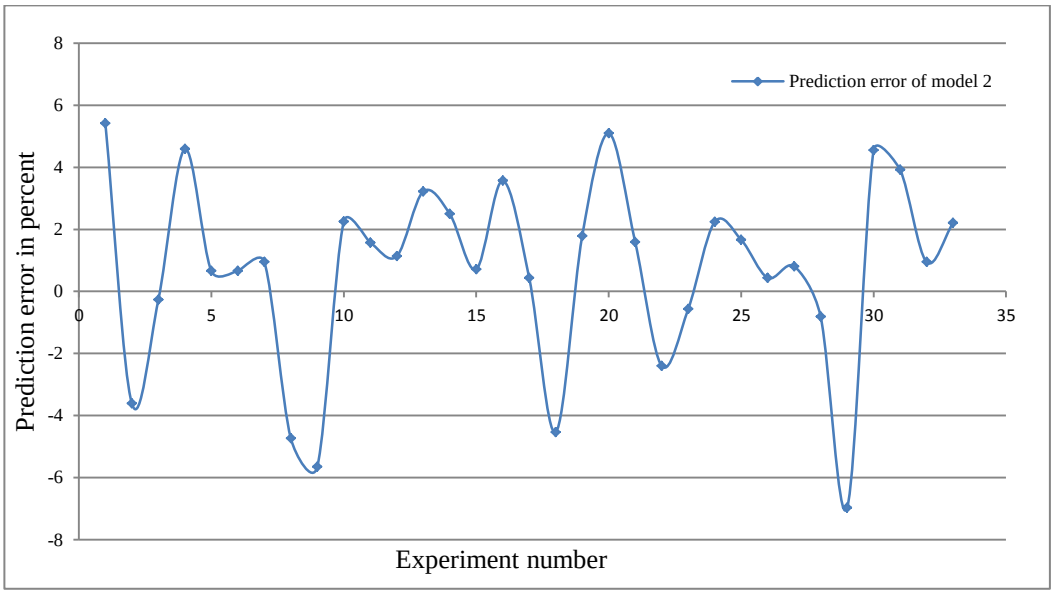

Figure 20: Prediction error of Model 2.

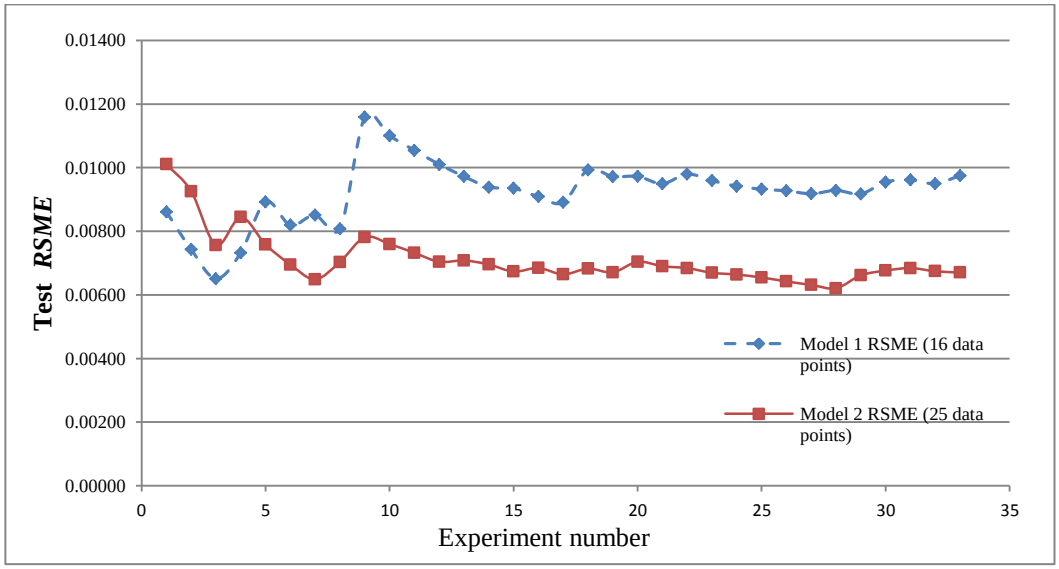

Figure 21: RSME of Models 1 & 2.

Following the procedure outlined in the flow chart, 18 optimization cycles were required to obtain the minimum drag coefficient with optimum parameters summarized in

Table 13. The optimized rear geometry for minimum drag is shown in Figure 23. The drag convergence history of optimized geometry is shown in Figure 24.

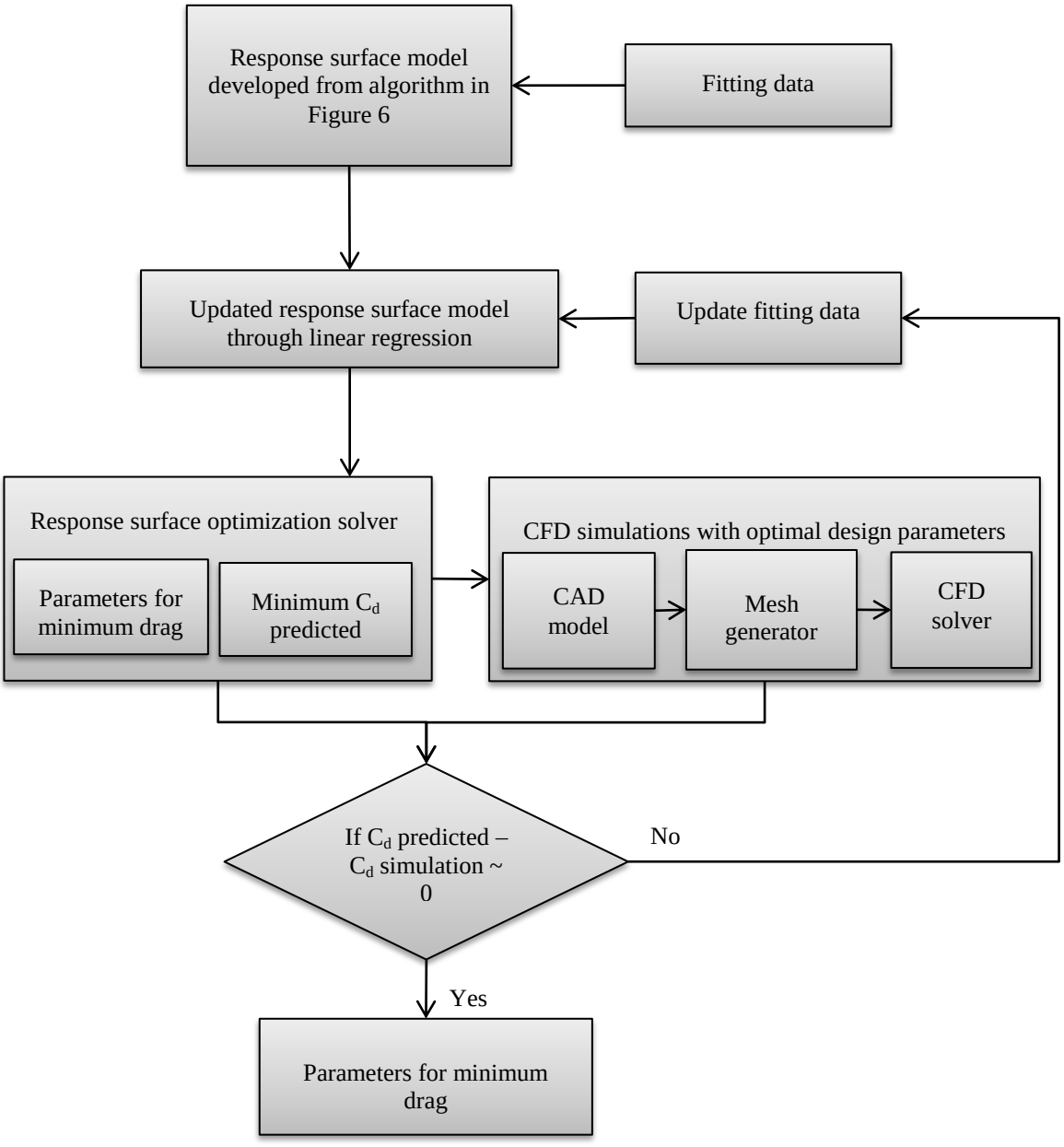

Figure 22: Work flow for optimization.

Table 13: Design parameters of notch back model for minimum drag.

NURBS parameters for minimum C_d					C_d
W_2	W_3	W_5	W_7	W_9	
0.623	2.875	0.000	0.100	0.000	0.186

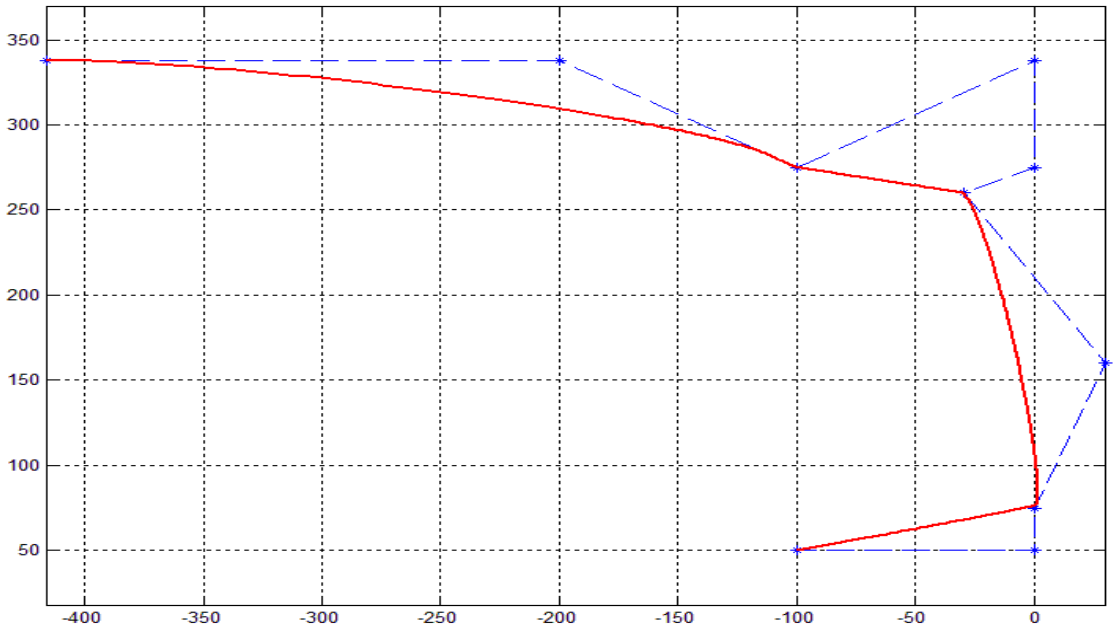

Figure 23: Rear geometry for minimum drag.

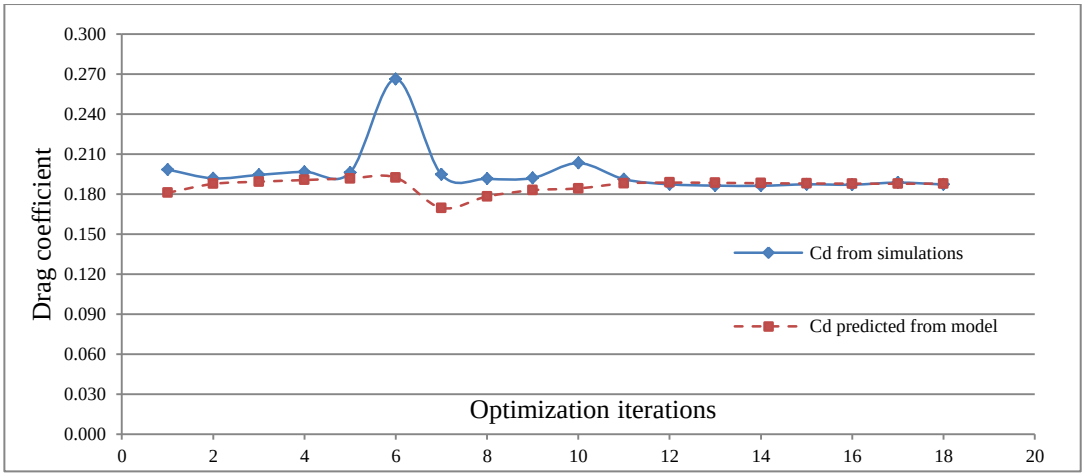

Figure 24: Drag convergence history.

Velocity streamlines and pressure contour around low drag geometry in Figure 25 show that the flow separates only at the slanted base and the diffuser geometry at bottom augments the pressure recovery. In case of high drag geometry obtained during the

optimization process, the flow separates at the top edge of the rear window and forms a large recirculation region in the wake as shown in Figure 26.

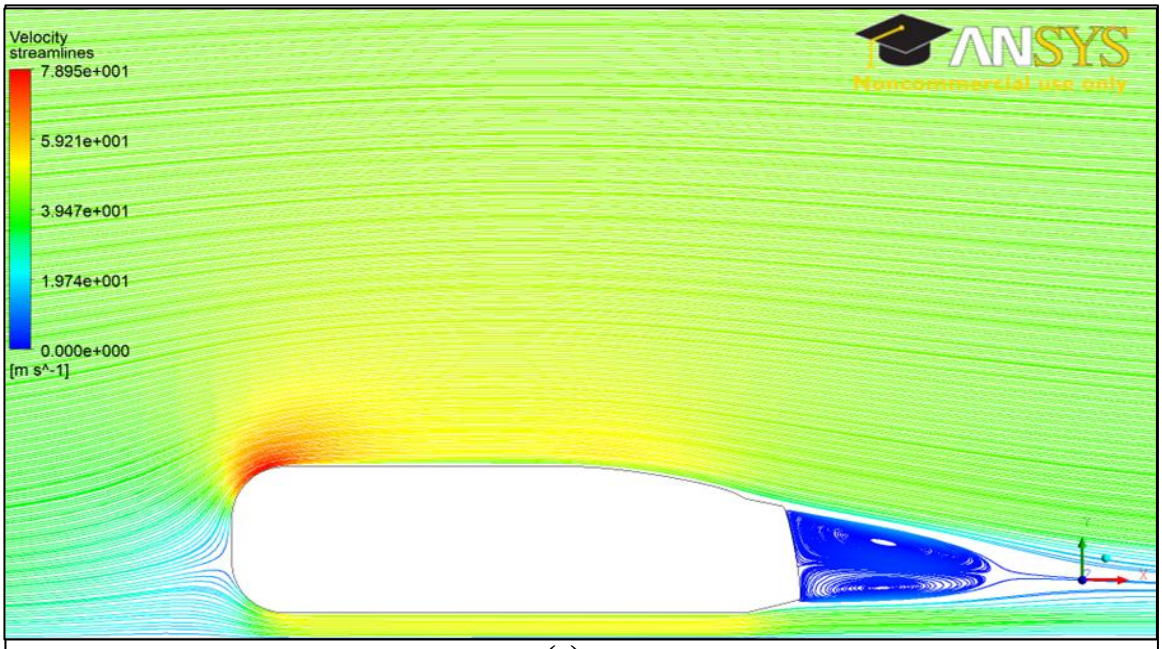

(a)

(b)

Figure 25: Velocity streamlines and pressure contour of minimum drag geometry. (a) Velocity streamlines, and (b) pressure contours.

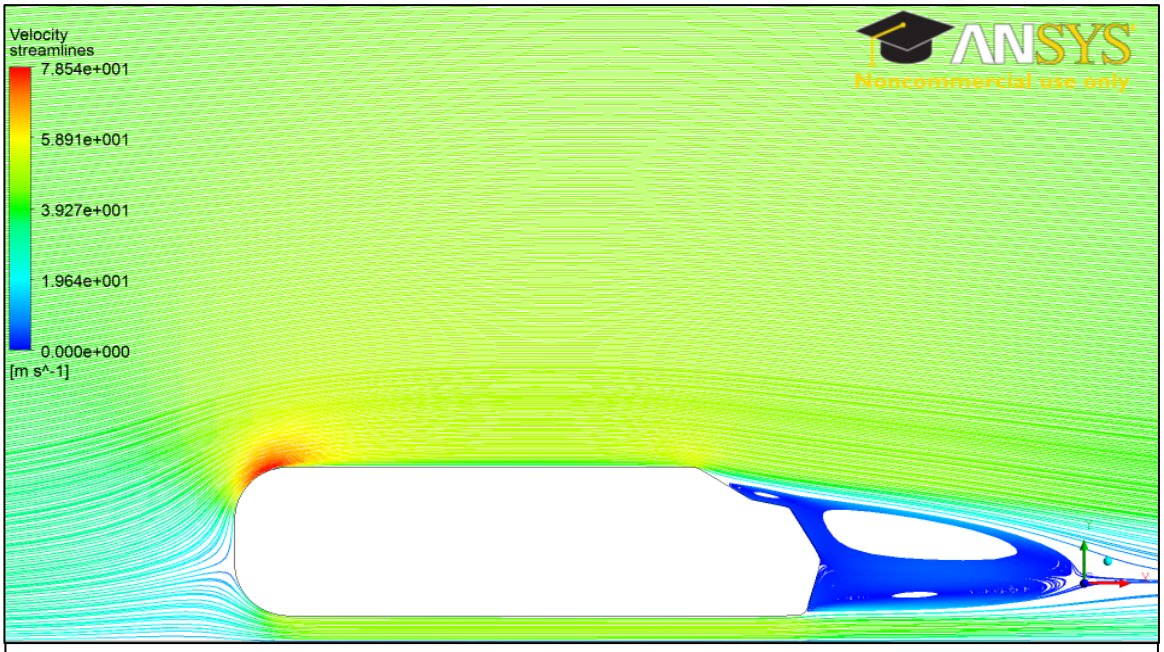

(a)

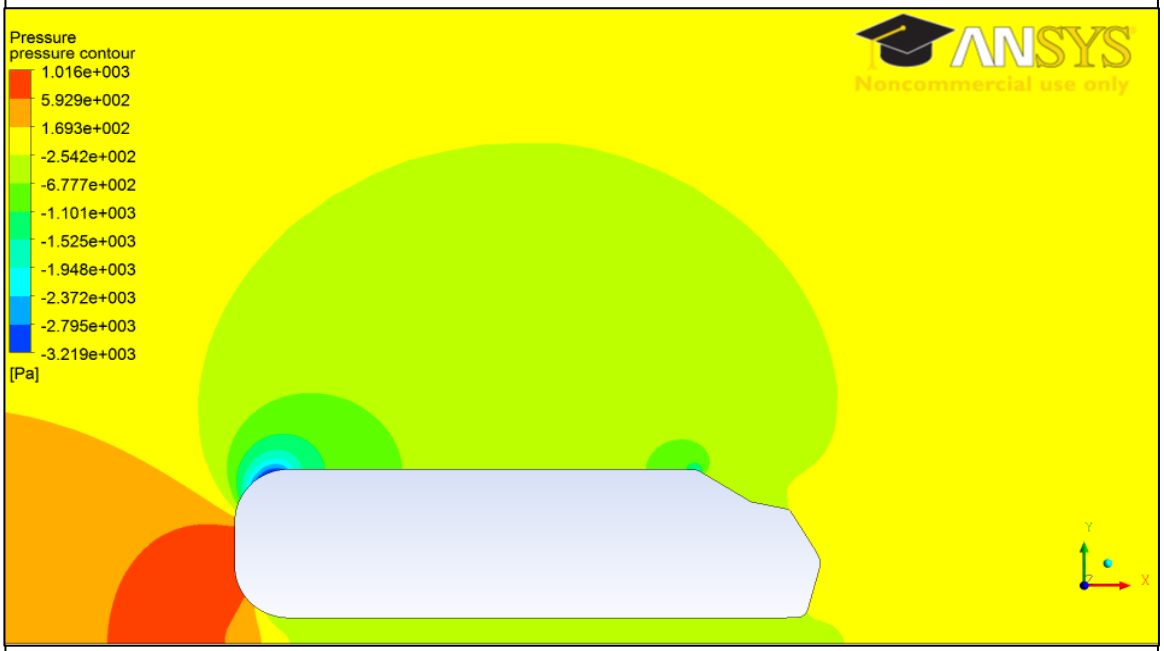

(b)

Figure 26: Velocity streamlines and pressure contour of high drag geometry. (a) Velocity streamlines, and (b) pressure contours.

Chapter 8: Conclusion and Future Work

8.1 Conclusion

The objective of this thesis was to develop a framework for passenger cars rear geometry parameterization and aerodynamic shape optimization. The geometric parameterization was implemented using NURBS parameters. This proposed technique greatly simplified the parameterization process. It also provided the flexibility to generate free form shapes which cannot be obtained using conventional parameterization techniques employed in automotive body design optimization. The study used the proposed parameterization technique to construct response surface models with NURBS parameters as the design variables. In addition, the aerodynamic drag of passenger cars was also related to NURBS parameters. The CFD was used to obtain aerodynamic drag for the construction of the response surface model. The advantage of using a response surface model in design optimization is that the model can predict the drag coefficient with a reasonable accuracy which eliminates the need to perform CFD simulations to evaluate each design.

The proposed technique was applied for aerodynamic design exploration of a simplified fast back model. The response surface of aerodynamic drag was constructed using three design parameters: the rear window slant, the base bulge and the diffuser geometry. The response surface model was able to predict the drag coefficient with a maximum error of 5% compared to the CFD simulation.

The framework developed in this thesis was also employed for the aerodynamic shape optimization of a simplified notch back model. The response surface method greatly simplified the optimization process since the parameters of minimum drag were predicted by the response surface and then CFD simulations were performed to verify the minimum drag. In this case, the response surface model of aerodynamic drag was constructed for five design variables. The optimization process required only 18 iterations to obtain the geometric parameters of minimum drag.

In conclusion, the proposed framework was implemented successfully. To the best of author's knowledge, this is the first time that NURBS have been used for car rear geometry aerodynamic shape optimization. The study also showed that response surface models can be used for design exploration and aerodynamic shape optimization. The work presented in this thesis will contribute significantly towards the aerodynamic development of passenger cars in the initial phase of design and enable the car designers and engineers to evaluate the aerodynamic performance of several vehicle shape designs cost effectively, quickly and efficiently.

8.2 Future work

Due to the large number of CFD simulations needed to be performed to test and validate the proposed framework, only two-dimensional car geometries were considered in this thesis. It is recommended that the proposed framework be implemented on three-dimensional vehicle geometries in future. In addition, the framework should be applied to more complex vehicle geometries such as sports utility vehicles and pickup trucks.

In the present study, neither the process of creating CAD models nor the construction of response surface models was fully automatic. Human intervention was required to create geometries based on design variables and also to construct response surface models at the end of the designed experiments. The efficiency of the proposed framework can be further enhanced by fully automating the two processes such that no human intervention is needed after setting up the parametric geometry.

References

Alvarez, L. (2000). Design optimization based on genetic programming. (Doctoral dissertation, University of Bradford, UK).

ANSYS® Academic Research, Release 13.0, Help System, Workbench user's guide, ANSYS, Inc.

ANSYS® Academic Research, Release 13.0, Help System, FLUENT Theory guide, ANSYS, Inc.

Bayraktar, I., Landman, D., and Baysal, O. (2001). Experimental and Computational Investigation of Ahmed Body for Ground Vehicle Aerodynamics. SAE Technical Paper 2001-01-2742.

Baker, C. A., Grossman, B., Haftka, R. T., Mason, W. H., & Watson, L. T. (1999). HSCT configuration design space exploration using aerodynamic response surface approximations. AIAA-98-4803.

Braus, M., Lanfrit, M. (2001). Simulation of the Ahmed Body. 9th ERCOFACT/IAHR Workshop on Refined Turbulence Modelling.

Bentamy, A., Trépanier, J. Y., & Guibault, F. (2002). Wing Shape Optimization Using a Constrained NURBS Surface Geometrical Representation. In ICAS Congress.

Cooper, K. R. (1993). Bluff body aerodynamics as applied to vehicles. Journal of Wind Engineering and Industrial Aerodynamics, 49, pp. 1-22.

Guo, L., Zhang, Y., & Shen, W. (2011). Simulation Analysis of Aerodynamics Characteristics of Different Two-Dimensional Automobile Shapes. Journal of Computers, 6(5), 999-1005. doi:10.4304/jcp.6.5.999-1005.

Gustavsson, T. (2006). Alternative approaches to rear end drag reduction. KTH, Department of Aeronautical and Vehicle Engineering, Royal Institute of Technology, TRITA-AVE 2006:12.

Hucho, W. H., & Sovran, G. (1993). Aerodynamics of road vehicles. Annual review of fluid mechanics. 25(1), 485-537.

H. Lienhart and S. Becker. (2003). Flow and turbulent structure in the wake of a simplified car model. SAE Paper 2003-01-0656, 2003.

Hu, X., Zhang, R., Ye, J., Yan, X., and Zhao, Z. (2011). Influence of Different Diffuser Angle on Sedan's Aerodynamic Characteristics. Physics Procedia, Volume 22, 2011, Pages 239-245.

Han, T., Hammond, D. C., and SAGI, C. J. (1992). Optimization of bluff body for minimum drag in ground proximity. AIAA Journal, Vol. 30, No. 4 (1992), pp. 882-889.

Kapadia, S., Roy, S. (2003). Detached Eddy Simulation over a reference Ahmed car model. AIAA Paper 2003-0857.

Keating, M. (2011). Accelerating CFD solutions. ANSYS Advantage magazine, Vol. V, issue 1.

Khuri, A. I., & Mukhopadhyay, S. (2010). Response surface methodology. 2010 John Wiley & Sons, Inc. WIREs Comp Stat 2010 2 128–149.

Krajnović, S. (2009). Optimization of aerodynamic properties of high-speed trains with CFD and response surface models. The Aerodynamics of Heavy Vehicles II: Trucks, Buses, and Trains, 197-211.

Krajnovi´c, S., and Davidson, L. (2004). Large-Eddy Simulation of the Flow Around Simplified Car Model. 2004 SAE World Congress, SAE Paper No. 2004-01-0227, Detroit, USA, 2004.

Lanfrit, M. (2005). Best practice guidelines for handling Automotive External Aerodynamics with FLUENT. (Version 1.2), Fluent Deutschland GmbH.

Lepine, J. Trépanier, J., Pepin, F. (2000). Wing Aerodynamic Optimization Using an Optimizied NURBS Geometrical Representation. AIAA-2000-0669.

Lavoie, P. (1999). An introduction to NURBS. Lecture notes.

Mayer, W., & Wickern, G. (2011). The New Audi A6/A7 Family-Aerodynamic Development of Different Body Types on One Platform. SAE International Journal of Passenger Cars-Mechanical Systems, 4(1), 197-206.

Mehta, U. B. (1991). Some aspects of uncertainty in computational fluid dynamics results. Journal of fluids engineering, 113(4), 538-543.

Morelli, A., Fioravanti, L., and Cogotti, A. (1976). The Body Shape of Minimum Drag. SAE Technical Paper 760186, 1976.

Morelli, A. (2000). A New Aerodynamic Approach to Advanced Automobile Basic Shapes. SAE Technical Paper 2000-01-0491.

Maji, S. and Almadi, H. (2007). Development of Aerodynamics of a Super Mileage Vehicle. SAE Technical Paper 2007-26-060, 2007, doi: 10.4271/2007-26-060.

Muyl, F., Dumas, L., & Herbert, V. (2004). Hybrid method for aerodynamic shape optimization in automotive industry. Computers & Fluids, 33(5), 849-858.

Myers, R. H., & Anderson-Cook, C. M. (2009). Response surface methodology: process and product optimization using designed experiments (Vol. 705). John Wiley & Sons.

Marjavaara, D. (2006). CFD driven optimization of hydraulic turbine draft tubes using surrogate models. (Doctoral dissertation, Division of Fluid Mechanics, Luleå University of Technology).

NURBS toolbox available at http://www.mathworks.com/matlabcentral/fileexchange/26390-nurbs-toolbox-by-d-m-spink.

Peterson, R.L. (1981). Drag reduction by the addition of a boat-tail to a box shaped vehicle. NASA contractor report 163113.

Peddiraju, P., Papadopoulous, A., Singh, R. (2009). CAE framework for aerodynamic design development of automotive vehicles. 3rd ANSA & μETA International Conference.

Piegl, L. A., & Tiller, W. (1997). The NURBS book. Springer Verlag.

Rogers, D. F. (2001). An introduction to NURBS: with historical perspective. Morgan Kaufmann Pub.

S. R. Ahmed, G. Ramm, and G. Faltin. (1984). Some salient features of the time averaged ground vehicle wake. SAE Paper 840300.

Song, W., & Keane, A. J. (2004). A study of shape parameterisation methods for airfoil optimisation. 10th AIAA/ISSMO Multidisciplinary Analysis and Optimization Conference (pp. 2031-2038).

Samareh, J. A. (2004). Aerodynamic shape optimization based on free-form deformation. AIAA, 4630.

Simpson, T. W., Poplinski, J. D., Koch, P. N., & Allen, J. K. (2001). Metamodels for computer-based engineering design: survey and recommendations. Engineering with computers, 17(2), 129-150.

Slater, J. W., (2008). Uncertainty and Error in CFD Simulations. Web link: http://www.grc.nasa.gov/WWW/wind/valid/tutorial/errors.html

Sobester, A., Leary, S. J., & Keane, A. J. (2004). A parallel updating scheme for approximating and optimizing high fidelity computer simulations. Structural and multidisciplinary optimization. 27(5), 371-383.